Cardiovascular disease risk factors induce mesenchymal features and senescence in cardiac endothelial cells

Karthik Amudhala Hemanthakumar[1,2], Fang Shentong[1,3], Andrey Anisimov[1,3], Mikko I. Mäyränpää[4], Eero Mervaala[5], Riikka Kivelä[1,2]

[1]Wihuri Research Institute, Helsinki, Finland

[2]Stem cells and Metabolism Research Program, Research Programs Unit, Faculty of Medicine, University of Helsinki, Helsinki, Finland

[3]Translational Cancer Medicine Research Program, Research Programs Unit, Faculty of Medicine, University of Helsinki, Helsinki, Finland

[4]Pathology, Helsinki University and Helsinki University Hospital, Helsinki, Finland

[5]Department of Pharmacology, Faculty of Medicine, University of Helsinki, Helsinki, Finland

Address for correspondence:

Dr. Riikka Kivelä, PhD

Stem cells and Metabolism Research Program

Research programs unit, Faculty of Medicine

University of Helsinki, PO Box 63, 00014 Helsinki, Finland

Tel: +358 2941 25516

Email: riikka.kivela@helsinki.fi

Abstract

Aging, obesity, hypertension and physical inactivity are major risk factors for endothelial dysfunction and cardiovascular disease (CVD). We applied fluorescence-activated cell sorting (FACS), RNA sequencing and bioinformatic methods to investigate the common effects of CVD risk factors on cardiac endothelial cells (ECs). Aging, obesity and pressure overload all upregulated pathways related to TGF-β signaling and mesenchymal gene expression, inflammation, vascular permeability, oxidative stress, collagen synthesis and cellular senescence, whereas exercise training downregulated most of the same pathways. We identified collagen chaperone SerpinH1/HSP47 to be significantly increased by aging and obesity and repressed by exercise training. Mechanistic studies demonstrated that SERPINH1/HSP47 in human ECs changed cell morphology and increased mesenchymal gene expression, while its silencing inhibited collagen deposition. Our data demonstrate that CVD risk factors significantly remodel the transcriptomic landscape of cardiac ECs to acquire senescence and mesenchymal features. SERPINH1/HSP47 was identified as a potential therapeutic target in ECs.

Keywords: Aging, Obesity, Exercise, Endothelium, Cellular reprogramming, Heart, TGF-β

Introduction

According to WHO, cardiovascular diseases (CVD) account for 10% of the global disease burden and constitute the number one cause of death in the Western world. CVD are mainly caused by behavioral (physical inactivity, unhealthy diet) and metabolic (obesity, hypertension, diabetes, high cholesterol) risk factors [1]. Aging, however, is by far the biggest contributor to CVD, and aging population is becoming an enormous challenge worldwide.

The heart contains a dense vascular network, and endothelial cells (EC) are indeed the most abundant cell population in the adult mouse heart [2]. In addition to their transport function, ECs are defined to control vasomotor tone, maintain vascular homeostasis, regulate angiogenesis, and to establish bidirectional communication with other cell types and organs via paracrine signaling mechanisms [3-7]. ECs are found to be highly adaptive to physiological stimuli during normal growth and development [8, 9], and the diversity of ECs in different tissues has now been acknowledged. ECs are also maladaptive to a spectrum of pathological events involving e.g. inflammation or oxidative stress [10, 11], and the development of heart diseases is strongly linked to endothelial dysfunction and impaired vascular remodeling. However, the molecular cues, which cause maladaptation and dysfunction of ECs in the heart in response to pathological signals, remain elusive.

Physical inactivity increases the incidence of several chronic diseases, whereas regular exercise training has positive effects on most of our tissues [12]. Because microcirculation is present in every organ in the body, ECs have a unique ability to influence the homeostasis and function of different tissues, and they are potentially a major cell type mediating the positive effects of exercise throughout the body. Although the cardiac benefits of exercise

are clear and there have been major advances in unraveling the molecular mechanisms, the understanding of how the molecular effects are linked to health benefits is still lacking [12]. Especially, the effects on ECs have not been characterized.

We hypothesized that the major CVD risk factors aging, obesity and pressure overload will induce adverse remodeling of cardiac EC transcriptome [11, 28, 29], whereas exercise training would provide beneficial effects [8, 9]. Both physiological and pathological stimuli significantly modified the cardiac EC transcriptome. Intriguinly, our results demonstrated that CVD risk factors promoted activation of transforming growth factor-β (TGF-β) signaling, cellular senecence and induced mesenchymal gene expression in cardiac EC, whereas exercise training promoted opposite protective effects.

Results

Exercise training and CVD risk factors modulate cardiac EC number, vascular density and transcriptome

To mimic the effect of the most common CVD risk factors (aging, obesity, pressure overload/hypertension and physical inactivity), we used adult C57BL/6J wild type mice in the following experimental groups: aged (18 months) vs. young (2 months) mice, high-fat diet induced obesity (14 weeks HFD) vs. lean mice, transverse aortic constriction (TAC) vs. sham-operated mice and exercise training (progressive treadmill running for 6 weeks) vs. sedentary mice (**Figure S1A-B**). Exercise trained mice showed improved ejection fraction compared to the sedentary mice, whereas aging, HFD and TAC resulted in impaired heart function (**Figure S1C-F and Supplementary Table 1**). HFD also induced marked weight gain, increased fat mass and impaired glucose tolerance (**Figure S1G-I**). Left ventricular (LV) mass was increased in aged, HFD-treated and TAC mice (**Supplementary Table 1**). Exercise training also slightly increased LV mass, which reflects mild physiological hypertrophy often observed in endurance-trained athletes [30] (**Supplementary Table 1**).

Exercise training significantly increased, whereas aging, HFD and TAC decreased the percentage, count and mean fluorescence intensity of the cardiac ECs ($CD31^+CD140a^-CD45^-Ter119^-DAPI^-$) compared to the controls, when analyzed by FACS (**Figure 1A-B, Figure S2A-D**). This was also demonstrated by immunohistochemistry for CD31-positive coronary vessels (**Figure 1C-D**). The cardiac ECs were gated and sorted by FACS (**Figure S3A**), and the isolated ECs were first analyzed by quantitative PCR analysis, which indicated significant enrichment of EC markers Cdh5 and Tie1 in the sorted fraction compared to whole heart or other cardiac mononuclear cells (**Figure S3B**). In addition,

isolation resulted in 87.4±1.9% cell viability and RNA purification strategy yielded intact and stable RNA with average RNA integrity number (RIN) of 8.7 (**Figure S3C-D**). RNA sequencing of isolated ECs was used to profile the expression pattern of cardiac EC transcripts in different experimental groups. Two-dimensional principal component analysis of the EC transcriptomes exhibited significant proportion of variance in the gene expression pattern, which can be attributed to the treatment-induced changes in cardiac EC transcriptome (**Figure S4A-E**). Notably, unsupervised hierarchical clustering of EC data sets for all experimental interventions (sedentary, exercise trained, young, aged, sham, TAC) revealed consistent clustering and high degree of similarity in the gene expression pattern (**Figure S4F-J**). The analysis for differentially expressed genes (DEGs) showed a large number of up- and downregulated genes especially in aged, obese and TAC-operated mice followed by a smaller number of affected genes in exercise trained mice. The number of significantly up- and downregulated genes with the false discovery rate 0.05 for each treatment are shown in the MA plots and the top 50 DEGs for each treatment are presented by heat maps (**Figure 2A-E, F-J**).

CVD risk factors induce senescence and TGF-β signaling together with mesenchymal gene expression in cardiac ECs

To understand biological functions of the differentially expressed genes (DEG), we used PANTHER classification analysis (**Figure 3A**). The analysis revealed that genes related to EC development, adherence junction organization, IGFR signaling, adrenomedullin receptor signaling, and mitochondria were upregulated by exercise training. Furthermore, exercise training downregulated pathways related to cellular aging, vascular membrane permeability, negative regulation of angiogenesis, TGF-β1 production, collagen activated tyrosine kinase signaling, and ossification. In contrast, pathways related to TGF-β, IFNα, TNFα, oxidative

stress, EC differentiation, vascular permeability, cell aging, collagen synthesis, SMAD signaling and mesenchymal cell development were highly enriched in cardiac EC from both aged and obese mice. Downregulated pathways in these mice included tissue and lipid homeostasis, ECM assembly, tube morphogenesis, cell adhesion, cell number maintenance, EC proliferation, vasculature development, artery development, and NOTCH signaling. Pressure overload activated pathways such as cellular response to TGF-βR2 activation of fibrotic pathways, inactivation of cell survival pathways Erk1/2 and MAPK, and ossification process, whereas cellular homeostasis and vasculature development were repressed.

Comparison of the GO biological terms, which were significantly affected by exercise training and the CVD risk factors, demonstrated clear opposite effects on the EC transcriptome. Aging and HFD promoted oxidative stress response, activation of inflammatory and fibrosis pathways and cellular aging, and inhibited pathways regulating cell number maintenance, proliferation and lipid homeostasis. Exercise training, in turn, promoted EC homeostasis and vascular growth, and prevented vascular aging, inflammation and pathological activation.

Because the gene ontology categories indicated upregulation of genes and pathways associated to mesenchymal development and endothelial-to-mesenchymal transition (EndMT) by CVD risk factors, we reviewed our differentially expressed gene sets for the expression of selected endothelial and mesenchymal markers based on the previously published data sets (**Supplementary Table 5A-E**). We found significant upregulation of many mesenchymal markers and downregulation of EC genes in aged and obese mice (**Figure 3C-D**). After two weeks of TAC, we also observed upregulation of several mesenchymal markers, whereas after seven weeks of TAC, there was both up- and

downregulation of the EC and mesenchymal markers, indicating possible reversal of the process (**Figure 3E-F**). Strikingly, exercise training downregulated several EndMT genes (Fscn1, Cd93, Vwa1, Sparc, Tuba1a, Cd44, Trp53, Col4a2, Mest, Cnn2, Tnfaip1, Lamb1, Ltbp4, Unc5b), the angiogenesis inhibitor gene Vash1, and the endothelial activation marker Apln and its receptor Aplnr, whereas it upregulated the expression of Malat1, Mgp, Krit1 and Calcrl (**Figure 3B**). We validated the results using an expanded set of samples by qPCR for Apln, Vim, Tgfbr2, Vash1, Sparc and Tgfb1 (**Figure S6A-F**).

SerpinH1 expression is increased by aging and obesity and repressed by exercise training

To identify genes, which could mediate the negative effect of aging and obesity and the protective effects of exercise, we performed gene overlap analysis of DEGs from these three experimental interventions. We found 4 genes significantly affected by all treatments, of which 2 genes (SerpinH1/Hsp47 and Vwa1) were upregulated by aging and HFD, and downregulated by exercise training. The other two genes (Mest and Fhl3) were upregulated by HFD and downregulated by exercise training and aging (**Figure 4A-C**). We performed an in silico secretome analysis to characterize the properties of the identified genes using MetaSecKB database (**Figure 4D**). Both SerpinH1 and Vwa1 contain a signal peptide for secretion, indicating they could act as angiocrines in autocrine and/or paracrine fashion.

We focused on SerpinH1/Hsp47, as it has a known role as a collagen chaperone and has been linked to fibrosis [31], making it an attractive candidate. We validated the endothelial SerpinH1/Hsp47 expression by qPCR (**Figure 4C**), and at single cell level using Tabula Muris database [32] and cardiac EC atlas from the Carmeliet lab [33]. The scRNAseq analysis revealed that SerpinH1 is expressed in variety of cell types within the mouse heart, including

fibroblasts, myofibroblasts, smooth muscle cells, endothelial cells, endocardial cells and to lesser extent in cardiomyocytes (**Figure S7A-D**). In ECs, SerpinH1 was found to be expressed throughout all endothelial cell clusters, with the highest expression in the apelin-high cluster marking activated ECs (**Figure S8A-F**). Interestingly, the expression of mesenchymal markers such as Tagln2, Vim and Smtn was also high in this cluster. Next, we analyzed the expression of SERPINH1/HSP47 in healthy human heart and in human cardiac ECs. Immunohistochemistry demonstrated SERPINH1/HSP47 to be highly expressed throughout the coronary vasculature and in fibroblasts in human heart, and weak staining was also detected in cardiomyocytes (**Figure 4E-G**, **Figure S7D**). In human cardiac ECs, HSP47 was localized perinuclearly, similarly to what has been demonstrated in other cells types, and consistent with the ER retention motif in its N-terminus (**Figure 4E**) [34-36]. We also tested, if exercise training can attenuate the expression of SerpinH1, Vwa1 and selected markers of TGF-β signaling/EndMT also in aged mice. Of the studied genes, mRNA expression of SerpinH1 and Vimentin were significantly repressed by exercise and there was a tendency also for Vwa1 (**Figure 4H-K**).

Overexpression of SERPINH1/HSP47 induces mesenchymal features in human ECs

To study the effects of SERPINH1/HSP47 in human ECs, we produced lentiviral vector encoding myc-tagged hSERPINH1/HSP47. Both human umbilical venous endothelial cells (HUVECs) and human cardiac arterial endothelial cells (HCAECs) were analyzed. HSP47 protein was localized similarly to the native protein (**Figure 5B**), and the overexpression was verified by western blotting (**Figure S9A**). Overexpression of HSP47 altered the cellular morphology characterized by impaired or discontinuous vascular endothelial cadherin junctions, increased stress fiber formation, and larger cell size (**Figure 5A-B**). Furthermore, analysis of EC and mesenchymal cell related transcripts demonstrated significant

repression of EC markers (CD31, CDH5, TIE1, NRARP, ID1) and induction of a proliferation gene CCND1, and mesenchymal/EndMT markers (TAGLN, aSMA, CD44, VIM, NOTCH3, ZEB2, SLUG, FN1, VCAM1, ICAM1) (**Figure 5C**). VE-cadherin downregulation was also confirmed at protein level (**Figure 5D**) and increased aSMA expression by immunofluorescence staining.

Transcriptomic changes pointed towards activated TGF-β signaling and oxidative stress in response to all of the CVD risk factors. Both are known to contribute to EC dysfunction and EndMT, thus we tested if they act as uptream regulators of HSP47. Indeed, our results show that TGF-β1 -treatment of HCAECs significantly upregulated the expression of SERPINH1 together with other known EndMT markers, and there was also small but significant induction of SERPINH1/HSP47 by hydrogen peroxide treatment (**Figure 5F**).

SERPINH1/HSP47 is needed for collagen 1 deposition by ECs

To investigate the significance of SERPINH1/HSP47 depletion in human cardiac ECs, HCAECs were transduced with four independent shSERPINH1 lentiviral constructs. The constructs induced approximately 80% deletion of mRNA (**Figure 6D**). The cell morphology was not affected after two days (**Figure 6A**), but ten days of silencing significantly changed endothelial cell morphology and decreased the cell density in culture (**Figure 6B**), suggesting that SERPINH1/HSP47 might play a role in EC homeostasis and function. SERPINH1 silencing significantly inhibited collagen fibril deposition, detected by immunistochemistry for type 1 collagen (**Figure 6B, C**). Only the cells transduced with the construct #1 could produce some extracellular collagen 1, and these cells also survived better than the cells transduced with constructs #2, #3 or #4 (**Figure 6B, C**). Next, we treated the cells with TGF-β1 and hydrogenperoxide for five days to induce EndMT features, as described previously [21, 37]. We used the shSERPINH1 (#1) construct, because from the other

silencing constructs not enough cells survived for the experiments. The results indicated that silencing of SERPINH1 prevented the appearance of Taglin-positive cells, a commonly used readout for EndMT, which were observed in the control cells (**Figure 6E**). We also studied the effect of SERPINH1/HSP47 on cell proliferation/migration. In the scratch wound healing assay, overexpression of SERPINH1 significantly promoted wound closure (**Figure 7A, B**), whereas silencing of SERPINH1 for two days significantly decreased EC proliferation/migration. (**Figure 7C, D**).

Discussion

Here we have used transcriptomic profiling to decipher how the major CVD risk factors aging, obesity and pressure overload remodel cardiac endothelial cells, and how the protective effects of exercise are mediated. The results demonstrate that the CVD risk factors activate transcriptional programs promoting cell aging, senescence, TGF-β activation, inflammation and oxidative stress in cardiac ECs. Importantly, exercise attenuated these same pathways, even in healthy mice. Furthermore, we found that aging, obesity and pressure overload induced mesenchymal gene programs in cardiac ECs, which can contribute to dysfunctional endothelium and CVD development. Analysis of potential disease-promoting genes identified SerpinH1/HSP47 to be induced by aging and obesity, while its expression was significantly repressed by exercise, even in old mice. Mechanistically, SERPINH1/HSP47 was induced by TGF-β and ROS, and the overexpression of SERPINH1/HSP47 increased cell size and stress fiber formation, weakened cell-cell junctions and promoted mesenchymal gene expression in human cardiac ECs. Immunohistochemistry of human hearts showed that HSP47 is abundantly expressed throughout the cardiac vasculature.

The largest dysregulation of the cardiac EC transcriptome was found in aged mice, followed by obesity and pressure overload. Exercise training affected a smaller number of transcripts, which can be accounted, at least partly, to the young and healthy control mice, which could move unrestrictedly in their home cages. Interestingly, however, most of the pathways activated by CVD risk factors were the same that were repressed by exercise training, highlighting the potential of physical activity to improve cardiovascular health via modulating endothelial cell phenotype and function. The positive effects of exercise on skeletal muscle

and cardiac angiogenesis have been described previously [38], but exercise-induced molecular changes in ECs have not been characterized. Aging and obesity, on the other hand, are known to contribute to capillary rarefaction and/or dysfunction [10, 11, 39, 40], and another novel aspect in this study was the comparison of several CVD risk factors to identify common pathways and genes, which could drive the pathogenesis in cardiac disease, and could be considered as potential therapeutic targets. ECs would provide an attractive target for drug development, as they are the first cells to encounter drugs in the bloodstream.

Dysfunctional endothelium likely contributes to more diseases than any other tissue in the body as it affects all organs. On the other hand, endothelium could act as an important mediator of the health-promoting effects of exercise in a variety of tissues. Our finding that aging, obesity and pressure overload induce mesenchymal gene programs in cardiac ECs adds to the increasing evidence that activated endothelial TGF-β signaling and acquisition of mesenchymal features play an important role in the development of EC dysfunction and cardiac diseases [13, 20, 41, 42]. Importantly, genes related to TGF-β production and cellular aging were repressed by exercise, highlighting the mechanisms behind the potential of exercise training in preventing and delaying the development of CVD. The activation of TGF-β signaling pathway has been implicated as a driving force for EndMT [21, 23-26]. Several studies have recently suggested that EndMT could contribute to the development of various cardiovascular diseases [16 13, 14, 27], but currently there is a lack of understanding of the causal relationships and mechanisms linking EndMT and CVD [13]. Furthermore, whether the transition from ECs to mesenchymal cells occurs completely in various CVDs is still actively debated in the literature. It has been suggested that pathological EC activation will result in acquired EndMT features e.g. expression of mesenchymal genes, without full transformation from one cell type to another [44]. This is in line with our findings, as only cells

with high CD31 expression and with no expression of CD45, CD140a and Ter119 were included in our analyses. Thus, all the analyzed cells were endothelial cells, but in the CVD risk factor groups they demonstrated increased mesenchymal marker expression. Long-term lineage tracing of ECs in response to CVD risk factors would provide further knowledge if and to what extent full transformation of ECs to mesenchymal cells occurs in cardiac vasculature. Our results, however, demonstrate that ECs acquire mesenchymal features due to CVD risk factors, which likely results in EC dysfunction even without EndMT.

To identify possible pathology-driving genes, which would be common for several risk factors, we performed gene overlap analysis using all data sets. Two genes, SerpinH1 and Vwa1, were found to be significantly increased by both aging and obesity and decreased by exercise, suggesting that they could act as common mediators of EC dysfunction. We focused in this study on Serpinh1/Hsp47, as it is a collagen chaperone and has been shown to contribute to tissue fibrosis [31, 45], an important feature of many cardiac diseases. Recently, it was demonstrated in a mouse pressure overload model using Hsp47 cell type -specific knockout mice that Hsp47 in myofibroblasts is an important regulator of pathologic cardiac fibrosis [45]. In line with our results in human cardiac ECs, collagen 1 production was decreased in the EC-specific Hsp47 deficient hearts [45]. In human ECs, our results placed SERPINH1/HSP47 downstream of TGF-β and ROS, and demonstrated that its overexpression promoted mesenchymal features in human cardiac EC. Furthermore, SERPINH1/HSP47 was found to be important for extracellular collagen 1 deposition and EC proliferation/migration. Silencing of SERPINH1 also prevented the TGF-β induced appearance of TAGLIN-positive cells in human cardiac EC, which is considered as a marker for EndMT [21, 37]. Based on the publicly available single-cell RNA sequencing data and immunohistochemistry of the human heart samples, SERPINH1/HSP47 is abundantly

expressed in all cardiac endothelial populations. For further translational impact, the role of endothelial SERPINH1/HSP47 in aged, obese and hypertensive human hearts needs to be determined.

In conclusion, our data demonstrate that the major CVD risk factors significantly remodel the cardiac EC transcriptome promoting cell senescence, oxidative stress, TGF-β signaling and mesenchymal gene features, whereas exercise training provided opposite and protective effects. SerpinH1/Hsp47 was identified as one of the downstream effectors of TGF-β, which could provide a novel therapeutic target in endothelial cells.

Materials and Methods

An expanded Methods section is available in the Supplementary material.

Mouse Models

The committee appointed by the district of southern Finland approved all the animal experiments. Male C57BL/6J 7-8- week adult wild type mice were purchased from Janvier Labs, the detailed information about the mouse models, experimental procedures and treatments used in this study are described in the Data Supplement. The following four experimental groups were studied: exercise vs. sedentary, aged (18 mo) vs. young (2 mo), high-fat diet fed vs. chow-fed mice, and transverse aortic constriction (TAC) for two and seven weeks vs. sham-operated mice. Female C57BL/6J wild type mice of 19-24 months old were used for a separate exercise training experiment in old mice. The cohort size (n) for each experiment are shown in the respective figures or figure legends.

Fluorescence-activated cell sorting of cardiac endothelial cells

The murine hearts were minced and incubated with 1mg/ml of collagenase type I, II and IV dissolved in DPBS containing 0.3mM $CaCl_2$ at 37°C for 25 min. DMEM supplemented with 10% heat inactivated FCS was added and the cell suspension was filtered through 70µm nylon strainer. The cells were incubated with Fc receptor blocking antibody (CD16/32) for five minutes and followed by CD31, CD140a, CD45, Ter119 antibodies for 30 minutes. The live cardiac endothelial cells were defined as $CD31^+$ $CD45^-$ $Ter119^-$ $CD140a^-$ $DAPI^-$ and the FACS Aria II (BD Biosciences) was used to gate, analyze and sort live cardiac endothelial

cells. Data was acquired using FACS DIVA v8.0.1 and analyzed with FlowJo v10.1. The workflow is presented in detail in the **Figure S3A**.

RNA seq data analysis of cardiac endothelial cells

FACS sorted cardiac ECs were homogenized using QIA shredder (Qiagen) and purified using RNeasy Plus Micro Kit (Qiagen). Prior to the library preparation step, RNA integrity and concentration of the samples were measured using Agilent Tape station and Qubit fluorescence assay, respectively. SMARTer Stranded Total RNA-Seq Kit V2 – Pico Input Mammalian (Takara Bio, USA) library preparation kit was used and 50M single end reads (1 x 75bp) were sequenced using illumina NextSeq 550 System. The sequenced reads were analyzed using Chipster high-throughput analysis software. The RNA sequencing data is deposited in GEO database, under the accession number GSE145263.

Gene Ontology, Pathway analysis, Gene overlap and in silico gene characterization

To understand the biological role of differentially expressed genes, we used PANTHER classification system. VENNY 2.1 analysis software was used to identify overlapping genes and in silico gene characterization was performed using MetazSecKB knowledgebase, TargetP2.0 and SecretomeP1.0 softwares.

Cell culture

Human cardiac arterial endothelial cells (HCAEC) or human umbilical vein endothelial cells (HUVEC) were transduced with lentiviral vectors (LV) encoding human SERPINH1-Myc overexpressing construct and four short hairpin gene silencing constructs for SERPINH1. The protocols for lentiviral vector production and gene transduction are explained in supplemental materials, and target sequences for shRNA constructs are listed in the

Supplementary Table 3. For EndMT induction in HCAEC, a previously published method using TGF-β and H_2O_2 was used [21, 37].

Immunohistochemistry, Real-Time Quantitative Polymerase chain reaction and Western Blotting

The detailed procedures for immunohistochemical stainings, western blotting and real-time qPCR are described in the Supplementary Materials and Methods section. Primer sequences for SYBR green and TaqMan real-time qPCR assays are listed in the **Supplementary Table 4**, and the antibodies used in immunohistochemistry and western blotting are listed in the **Supplementary Table 2**.

Statistics

The data from the individual experiments were analyzed by student's *t* test. $P<0.05$ value was considered statistically significant and P values in the graphs are mentioned as *$P<0.05$, **$P<0.01$ and ***$P<0.001$. The data is shown as mean ± SEM. The GraphPad Prism 7 software was used for statistical analysis. Statistics used for RNA sequencing data are described in detail in the Supplementary materials.

Funding

We thank the Jenny and Antti Wihuri Foundation, Academy of Finland (RK, 297245), the Finnish Foundation for Cardiovascular Research (RK, KAH), the Sigrid Jusélius Foundation (RK), the Finnish Cultural Foundation (RK), The Finnish Medical Foundation (MIM), Biomedicum Helsinki Foundation (KAH) and Aarne Koskelo Foundation (KAH).

Acknowledgements

We would like to thank Dr. Ralf Adams and Dr. Guillermo Luxán for their help in setting up the EC isolation. Dr. Seppo Kaijalainen for cloning the SERPINH1/HSP47 overexpression vector. Kirsi Mattinen, Päivi Leinikka, Maria Arrano de Kivikko, Ilse Paetau, Tanja Laakkonen and Tapio Tainola for their excellent technical help. We thank the Laboratory Animal Center, the Biomedicum Imaging Unit, the HiLife Flow Cytometry Unit, the Biomedicum Functional Genomics Unit, and the AAV Gene Transfer and Cell Therapy Core Facility for the help and facilities.

Author contribution

KAH, EM and RK designed and KAH performed the experiments. KAH, SF, AA and RK analyzed the data. MIM collected the human heart samples. KAH and RK wrote the manuscript. All authors have seen, commented and accepted the manuscript.

Competing interests

No competing interests.

References

1.Mendis, S., Puska, P. & Norrving, P editors. Global Atlas on cardiovascular disease prevention and control. World Health Organization, Geneva, ISBN 978 92 4 156437 3 (2011).

2.Pinto AR, Ilinykh A, Ivey MJ, Kuwabara JT, D'Antoni ML, Debuque R, Chandran A, Wang L, Arora K, Rosenthal NA and Tallquist MD. Revisiting Cardiac Cellular Composition. *Circ Res*. 2016;118:400-9.

3.Aird WC. Phenotypic heterogeneity of the endothelium: I. Structure, function, and mechanisms. *Circ Res*. 2007;100:158-73.

4.Aird WC. Endothelial cell heterogeneity. *Cold Spring Harb Perspect Med*. 2012;2:a006429.

5.Kivela R, Hemanthakumar KA, Vaparanta K, Robciuc M, Izumiya Y, Kidoya H, Takakura N, Peng X, Sawyer DB, Elenius K, Walsh K and Alitalo K. Endothelial Cells Regulate Physiological Cardiomyocyte Growth via VEGFR2-Mediated Paracrine Signaling. *Circulation*. 2019;139:2570-2584.

6.Talman V and Kivela R. Cardiomyocyte-Endothelial Cell Interactions in Cardiac Remodeling and Regeneration. *Front Cardiovasc Med*. 2018;5:101.

7.Hemanthakumar KA and Kivela R. Angiogenesis and angiocrines regulating heart growth. *VascularBiology*. 2020; DOI:https://doi.org/10.1530/VB-20-0006.

8.White FC, Bloor CM, McKirnan MD and Carroll SM. Exercise training in swine promotes growth of arteriolar bed and capillary angiogenesis in heart. *J Appl Physiol (1985)*. 1998;85:1160-8.

9.Bloor CM. Angiogenesis during exercise and training. *Angiogenesis*. 2005;8:263-71.

10.Cines DB, Pollak ES, Buck CA, Loscalzo J, Zimmerman GA, McEver RP, Pober JS, Wick TM, Konkle BA, Schwartz BS, Barnathan ES, McCrae KR, Hug BA, Schmidt AM and Stern

DM. Endothelial cells in physiology and in the pathophysiology of vascular disorders. *Blood*. 1998;91:3527-61.

11.Gimbrone MA, Jr. and Garcia-Cardena G. Endothelial Cell Dysfunction and the Pathobiology of Atherosclerosis. *Circ Res*. 2016;118:620-36.

12.Hawley JA, Hargreaves M, Joyner MJ and Zierath JR. Integrative biology of exercise. *Cell*. 2014;159:738-49.

13.Kovacic JC, Dimmeler S, Harvey RP, Finkel T, Aikawa E, Krenning G and Baker AH. Endothelial to Mesenchymal Transition in Cardiovascular Disease: JACC State-of-the-Art Review. *J Am Coll Cardiol*. 2019;73:190-209.

14.Li Y, Lui KO and Zhou B. Reassessing endothelial-to-mesenchymal transition in cardiovascular diseases. *Nat Rev Cardiol*. 2018;15:445-456.

15.Eisenberg LM and Markwald RR. Molecular regulation of atrioventricular valvuloseptal morphogenesis. *Circ Res*. 1995;77:1-6.

16.Zeisberg EM, Tarnavski O, Zeisberg M, Dorfman AL, McMullen JR, Gustafsson E, Chandraker A, Yuan X, Pu WT, Roberts AB, Neilson EG, Sayegh MH, Izumo S and Kalluri R. Endothelial-to-mesenchymal transition contributes to cardiac fibrosis. *Nat Med*. 2007;13:952-61.

17.Zeisberg EM, Potenta SE, Sugimoto H, Zeisberg M and Kalluri R. Fibroblasts in kidney fibrosis emerge via endothelial-to-mesenchymal transition. *J Am Soc Nephrol*. 2008;19:2282-7.

18.Rieder F, Kessler SP, West GA, Bhilocha S, de la Motte C, Sadler TM, Gopalan B, Stylianou E and Fiocchi C. Inflammation-induced endothelial-to-mesenchymal transition: a novel mechanism of intestinal fibrosis. *Am J Pathol*. 2011;179:2660-73.

19.Maddaluno L, Rudini N, Cuttano R, Bravi L, Giampietro C, Corada M, Ferrarini L, Orsenigo F, Papa E, Boulday G, Tournier-Lasserve E, Chapon F, Richichi C, Retta SF,

Lampugnani MG and Dejana E. EndMT contributes to the onset and progression of cerebral cavernous malformations. *Nature*. 2013;498:492-6.

20.Chen PY, Qin L, Baeyens N, Li G, Afolabi T, Budatha M, Tellides G, Schwartz MA and Simons M. Endothelial-to-mesenchymal transition drives atherosclerosis progression. *J Clin Invest*. 2015;125:4514-28.

21.Evrard SM, Lecce L, Michelis KC, Nomura-Kitabayashi A, Pandey G, Purushothaman KR, d'Escamard V, Li JR, Hadri L, Fujitani K, Moreno PR, Benard L, Rimmele P, Cohain A, Mecham B, Randolph GJ, Nabel EG, Hajjar R, Fuster V, Boehm M and Kovacic JC. Endothelial to mesenchymal transition is common in atherosclerotic lesions and is associated with plaque instability. *Nat Commun*. 2016;7:11853.

22.Hulshoff MS, Xu X, Krenning G and Zeisberg EM. Epigenetic Regulation of Endothelial-to-Mesenchymal Transition in Chronic Heart Disease. *Arterioscler Thromb Vasc Biol*. 2018;38:1986-1996.

23.Cooley BC, Nevado J, Mellad J, Yang D, St Hilaire C, Negro A, Fang F, Chen G, San H, Walts AD, Schwartzbeck RL, Taylor B, Lanzer JD, Wragg A, Elagha A, Beltran LE, Berry C, Feil R, Virmani R, Ladich E, Kovacic JC and Boehm M. TGF-beta signaling mediates endothelial-to-mesenchymal transition (EndMT) during vein graft remodeling. *Sci Transl Med*. 2014;6:227ra34.

24.James D and Rafii S. Maladapted endothelial cells flip the mesenchymal switch. *Sci Transl Med*. 2014;6:227fs12.

25.Bischoff J. Endothelial-to-Mesenchymal Transition. *Circ Res*. 2019;124:1163-1165.

26.Bischoff J, Casanovas G, Wylie-Sears J, Kim DH, Bartko PE, Guerrero JL, Dal-Bianco JP, Beaudoin J, Garcia ML, Sullivan SM, Seybolt MM, Morris BA, Keegan J, Irvin WS, Aikawa E and Levine RA. CD45 Expression in Mitral Valve Endothelial Cells After Myocardial Infarction. *Circ Res*. 2016;119:1215-1225.

27.Sanchez-Duffhues G, Garcia de Vinuesa A and Ten Dijke P. Endothelial-to-mesenchymal transition in cardiovascular diseases: Developmental signaling pathways gone awry. *Dev Dyn*. 2018;247:492-508.

28.Ungvari Z, Tarantini S, Kiss T, Wren JD, Giles CB, Griffin CT, Murfee WL, Pacher P and Csiszar A. Endothelial dysfunction and angiogenesis impairment in the ageing vasculature. *Nat Rev Cardiol*. 2018;15:555-565.

29.Brandes RP. Endothelial dysfunction and hypertension. *Hypertension*. 2014;64:924-8.

30.Arbab-Zadeh A, Perhonen M, Howden E, Peshock RM, Zhang R, Adams-Huet B, Haykowsky MJ and Levine BD. Cardiac remodeling in response to 1 year of intensive endurance training. *Circulation*. 2014;130:2152-61.

31.Ito S and Nagata K. Roles of the endoplasmic reticulum-resident, collagen-specific molecular chaperone Hsp47 in vertebrate cells and human disease. *J Biol Chem*. 2019;294:2133-2141.

32.Tabula Muris C, Overall c, Logistical c, Organ c, processing, Library p, sequencing, Computational data a, Cell type a, Writing g, Supplemental text writing g and Principal i. Single-cell transcriptomics of 20 mouse organs creates a Tabula Muris. *Nature*. 2018;562:367-372.

33.Kalucka J, de Rooij L, Goveia J, Rohlenova K, Dumas SJ, Meta E, Conchinha NV, Taverna F, Teuwen LA, Veys K, Garcia-Caballero M, Khan S, Geldhof V, Sokol L, Chen R, Treps L, Borri M, de Zeeuw P, Dubois C, Karakach TK, Falkenberg KD, Parys M, Yin X, Vinckier S, Du Y, Fenton RA, Schoonjans L, Dewerchin M, Eelen G, Thienpont B, Lin L, Bolund L, Li X, Luo Y and Carmeliet P. Single-Cell Transcriptome Atlas of Murine Endothelial Cells. *Cell*. 2020;180:764-779 e20.

34.Masuda H, Fukumoto M, Hirayoshi K and Nagata K. Coexpression of the collagen-binding stress protein HSP47 gene and the alpha 1(I) and alpha 1(III) collagen genes in carbon tetrachloride-induced rat liver fibrosis. *J Clin Invest*. 1994;94:2481-8.

35.Razzaque MS, Hossain MA, Kohno S and Taguchi T. Bleomycin-induced pulmonary fibrosis in rat is associated with increased expression of collagen-binding heat shock protein (HSP) 47. *Virchows Arch*. 1998;432:455-60.

36.Honzawa Y, Nakase H, Shiokawa M, Yoshino T, Imaeda H, Matsuura M, Kodama Y, Ikeuchi H, Andoh A, Sakai Y, Nagata K and Chiba T. Involvement of interleukin-17A-induced expression of heat shock protein 47 in intestinal fibrosis in Crohn's disease. *Gut*. 2014;63:1902-12.

37.Magenta A, Cencioni C, Fasanaro P, Zaccagnini G, Greco S, Sarra-Ferraris G, Antonini A, Martelli F and Capogrossi MC. miR-200c is upregulated by oxidative stress and induces endothelial cell apoptosis and senescence via ZEB1 inhibition. *Cell Death Differ*. 2011;18:1628-39.

38.Hudlicka O, Brown M and Egginton S. Angiogenesis in skeletal and cardiac muscle. *Physiol Rev*. 1992;72:369-417.

39.Lopez-Otin C, Blasco MA, Partridge L, Serrano M and Kroemer G. The hallmarks of aging. *Cell*. 2013;153:1194-217.

40.Ungvari Z, Kaley G, de Cabo R, Sonntag WE and Csiszar A. Mechanisms of vascular aging: new perspectives. *J Gerontol A Biol Sci Med Sci*. 2010;65:1028-41.

41.Chen PY, Qin L, Li G, Wang Z, Dahlman JE, Malagon-Lopez J, Gujja S, Cilfone NA, Kauffman KJ, Sun L, Sun H, Zhang X, Aryal B, Canfran-Duque A, Liu R, Kusters P, Sehgal A, Jiao Y, Anderson DG, Gulcher J, Fernandez-Hernando C, Lutgens E, Schwartz MA, Pober JS, Chittenden TW, Tellides G and Simons M. Endothelial TGF-beta signalling drives vascular inflammation and atherosclerosis. *Nat Metab*. 2019;1:912-926.

42.Xiong J, Kawagishi H, Yan Y, Liu J, Wells QS, Edmunds LR, Fergusson MM, Yu ZX, Rovira, II, Brittain EL, Wolfgang MJ, Jurczak MJ, Fessel JP and Finkel T. A Metabolic Basis for Endothelial-to-Mesenchymal Transition. *Mol Cell*. 2018;69:689-698 e7.

43.Manavski Y, Lucas T, Glaser SF, Dorsheimer L, Gunther S, Braun T, Rieger MA, Zeiher AM, Boon RA and Dimmeler S. Clonal Expansion of Endothelial Cells Contributes to Ischemia-Induced Neovascularization. *Circ Res*. 2018;122:670-677.

44.Chen PY, Schwartz MA and Simons M. Endothelial-to-Mesenchymal Transition, Vascular Inflammation, and Atherosclerosis. *Front Cardiovasc Med*. 2020;7:53.

45.Khalil H, Kanisicak O, Vagnozzi RJ, Johansen AK, Maliken BD, Prasad V, Boyer JG, Brody MJ, Schips T, Kilian KK, Correll RN, Kawasaki K, Nagata K and Molkentin JD. Cell-specific ablation of Hsp47 defines the collagen-producing cells in the injured heart. *JCI Insight*. 2019;4:e128722.

46.Nagai N, Hosokawa M, Itohara S, Adachi E, Matsushita T, Hosokawa N and Nagata K. Embryonic lethality of molecular chaperone hsp47 knockout mice is associated with defects in collagen biosynthesis. *J Cell Biol*. 2000;150:1499-506.

Figure legends

Figure 1. Effects of exercise training, aging, obesity and pressure overload on cardiac endothelial cell number and vascular density. A-B. FACS analysis and quantification of mean fluorescence intensity (MFI) of the cardiac endothelial cells (CD31+CD140a-CD45-Ter119-DAPI-) in various mice models. **C-D.** Representative immunofluorescence images and quantification of CD31+ blood vessel area (%) in the heart. Scale bar, 100μm. Data is presented as mean ± SEM. Student's t test was used, *p<0.05, **p<0.01, ***p<0.001 (N=3-5 mice/group). In the panel **B**, each color-coded circle (Red, Green and Black) indicates an individual biological sample. In panel **D**, number of mice in each experimental group are indicated in the respective graph, N=3-5 mice/group.

Figure 2. Transcriptomic changes in cardiac endothelial cells from exercise trained, aged, obese and TAC-treated mice. A-E. MA (log ratio over mean) plots showing the number of differentially expressed genes in cardiac ECs for each experiment. Number of significantly up- and downregulated genes with the FDR (Benjamini-Hochberg adjusted pvalue) threshold of 0.05 are indicated in the plots. **F-J.** Top 50 differentially expressed genes in cardiac ECs of the indicated experimental groups. In the heatmap, each color-coded circle (Red, Green and Black) indicates an individual biological sample within each experimental group. N=3-4 mice/group.

Figure 3. Cardiovascular disease risk factors activate mesenchymal gene expression in cardiac ECs. A. Gene ontology analysis of the up- and downregulated genes. Note the opposite changes by exercise training compared to the CVD risk factors. **B-F.** Heatmaps showing the differential gene expression of endothelial and mesenchymal genes previously

associated to endothelial-to-mesenchymal transition (EndMT). Genes are selected based on published datasets (references are found in the supplementary table 5A-E). In the figure panel A-F, the up- and downregulated genes with the FDR (Benjamini-Hochberg adjusted pvalue) threshold of 0.05 were considered. In the heatmap, each color-coded circle (Red, Green and Black) indicates an individual biological sample within each experimental group. N=3-4 mice/group.

Figure 4. SerpinH1 expression is increased by aging and obesity and repressed by exercise training. A. Venn diagram showing the overlap of differentially expressed genes between the experiments. Four genes were identified to be significantly affected by aging, obesity and exercise (SerpinH1, Vwa1, Mest and Fhl3). **B.** Bar plot showing the expression pattern of these four genes. In panel **A** and **B**, the up- and downregulated genes with the FDR (Benjamini-Hochberg adjusted p-value) threshold of 0.05 were considered to be significant (N=3-4 mice/group). **C.** qPCR Validation of SerpinH1 and Vwa1 normalized to HPRT1 (N=4-6 mice/group). **D.** In silico secretome analysis of the identified genes. E-G. Representative immunofluorescent and immunohistochemistry images showing the expression of SERPINH1/HSP47 in human EC and human heart samples (red arrow head in the bottom panel F indicates the expression in large vessels and “L” indicate vessel lumen. White arrowheads in the panel G denote the co-expression of HSP47 and CDH5 in coronary vessels (yellow signal). **H-K.** mRNA expression of SerpinH1, Vwa1, Vim and Tgfbr2 in the cardiac ECs of sedentary and exercise trained aged mice (N=4-5/group). Scale bar 100 μm. Data is presented as mean ± SEM. Student’s t test was used, *p<0.05, **p<0.01, ***p<0.001.

Figure 5. Overexpression of SERPINH1 modifies the EC phenotype and induces mesenchymal gene expression in human cardiac ECs. A. Representative phase-

contrast images of live human cardiac arterial EC (HCAEC) transduced with LV-CTRL and LV-SERPINH1-Myc and quantification of the aspect ratio (length to width ratio) of the cell. **B.** Representative immunofluorescent images showing the expression of Myc-tagged SERPINH1 in green, F-Actin in grey and CDH5/VE-Cadherin in red. The insert within the white box shows magnified view of VE-Cadherin junctions in HCAECs. **C.** qPCR analysis of endothelial and mesenchymal markers in SERPINH1 overexpressing cells. **D.** Western blot analysis and quantification of CDH5/VE-cadherin expression in the SERPINH1 overexpressing HCAECs (normalized to GAPDH). **E.** Representative immunofluorescent images showing DAPI in blue, CDH5/VE-Cadherin in green and α-smooth muscle actin (aSMA) in red. **F.** qPCR analysis of SERPINH1 and EndMT markers in HCAECs stimulated with TGF-β1 (50ng/ml) or H_2O_2 for five days. In panel **A, C, D** and **F**, N=3 biological replicates/group were analyzed. Scale bar 100 μm. Data is presented as mean ± SEM. Student's t test was used, *p<0.05, **p<0.01, ***p<0.001.

Figure 6. SERPINH1/HSP47 silencing in human cardiac EC inhibits collagen production and secretion. **A.** Representative phase contrast images of live HCAECs transduced with LV-SCR and LV-shSERPINH1 (#1 and #2) and quantification of the aspect ratio (length to width ratio) of the cells after two days of silencing. **B.** Representative CDH5/VE-Cadherin immunofluorescent images (green) showing the cell morphology and density after ten days of SERPINH1 silencing. Collagen 1 staining is shown in red, and quantification of Collagen 1 is shown in **C**. **D.** qPCR analysis of SERPINH1 deletion levels using four independent constructs. **E.** Representative immunofluorescent images showing TAGLN expression in the control and SERPINH1 silenced HCAECs treated with recombinant human TGF-β1 with and without H_2O_2 for five days. In the panel **A, C** and **D**,

N=3 biological replicates/group were analyzed. Scale bar 100 μm. Data is presented as mean ± SEM. Student's t test was used, *p<0.05, **p<0.01, ***p<0.001.

Figure 7. SERPINH1 overexpression enhances and silencing inhibits wound closure in vitro. A-B. Representative phase contrast images of scratch wound healing assay performed in HCAECs treated with LV-CTRL and LV-SERPINH1, and quantification of the wound closure (%) with respect to time (hours). **C-D.** Representative phase contrast images of scratch wound healing assay performed in HCAECs treated with LV-SCR and LV-shSERPINH1 (#1 and #2), and quantification of the wound closure (%) with respect to time (hours). In the panel A and C, the blue area within the white dotted region indicate the wound area. In the panel **B** and **D**, N=8 biological replicates/group were analyzed. Data is presented as mean ± SEM. Student's t test was used, *p<0.05, **p<0.01, ***p<0.001.

Graphical abstract demonstrating the cardiovascular disease risk factor mediated activation of TGF-β signaling and acquisition of mesenchymal features in cardiac EC. CVD risk factors aging, obesity and pressure overload trigger the regression of coronary vasculature by activating TGF-β/ROS signaling pathways and cellular senescence. These induce the expression of SerpinH1/Hsp47 and mesenchymal gene signature. SerpinH1/Hsp47 and EndMT are both involved in the development of tissue fibrosis by increasing collagen deposition in the extracellular matrix. Exercise training, in turn, increases coronary vasculature density, EC number and represses TGF-β signaling, mesenchymal gene expression and senescence related pathways.

Figure 1

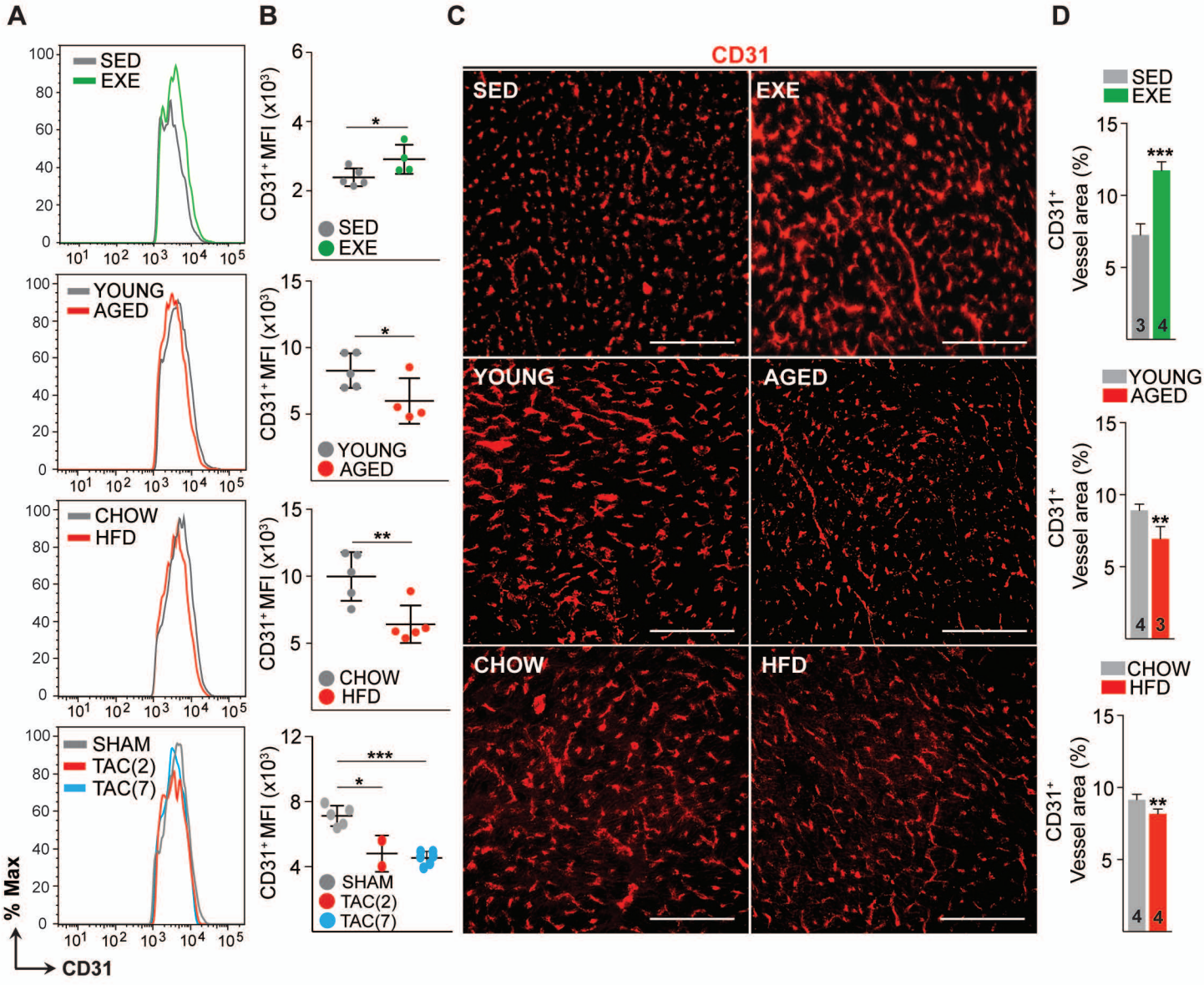

Figure 1. Effects of exercise training, aging, obesity and pressure overload on cardiac endothelial cell number and vascular density. A-B. FACS analysis and quantification of mean fluorescence intensity (MFI) of the cardiac endothelial cells (CD31+CD140a-CD45-Ter119-DAPI-) in various mice models. **C-D.** Representative immunofluorescence images and quantification of CD31+ blood vessel area (%) in the heart. Scale bar, 100 μm. Data is presented as mean ± SEM. Student's t test was used, *p<0.05, **p<0.01, ***p<0.001 (In the panel **B**, each color-coded circle (Red, Green and Black) indicates an individual biological sample. In panel **D**, number of mice in each experimental group are indicated in the respective graph, N=3-5 mice/group).

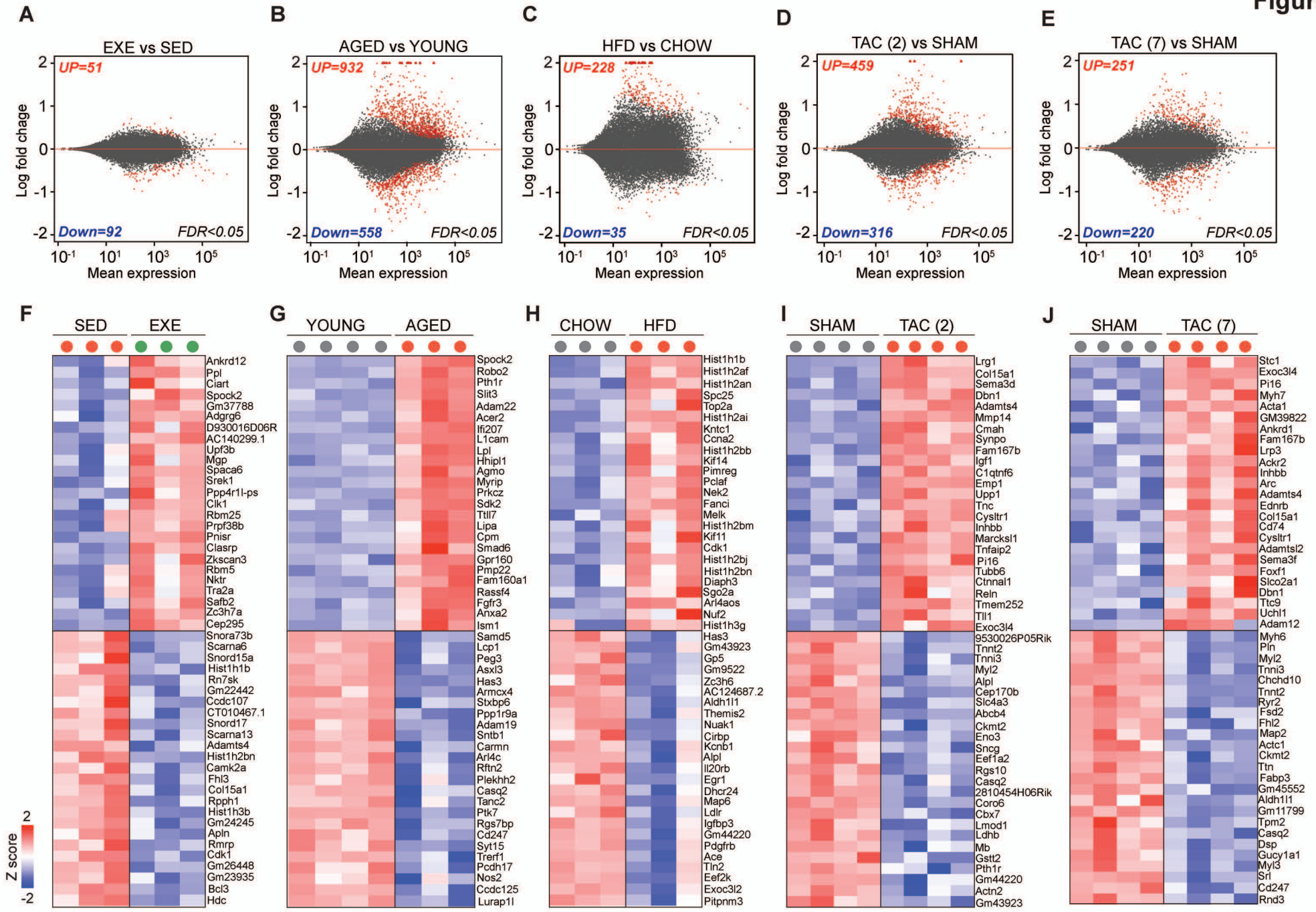

Figure 2. Transcriptomic changes in cardiac endothelial cells from exercise trained, aged, obese and TAC-treated mice. A-E. MA (log ratio over mean) plots showing the number of differentially expressed genes in cardiac ECs for each experiment. Number of significantly up- and downregulated genes with the FDR (Benjamini-Hochberg adjusted pvalue) threshold of 0.05 are indicated in the plots. **F-J.** Top 50 differentially expressed genes in cardiac ECs of the indicated experimental groups. In the heatmap, each color coded circle (Red, Green and Black) indicates an individual biological sample within each experimental group. N=3-4 mice/group.

Figure 3

A

	Exercise training		Aging or HFD		TAC	
	Gene ontology	-log(p)	Gene ontology	-log(p)	Gene ontology	-log(p)
Upregulated	Epithelial cell development	2.14	Endothelial cell differentiation	9.55	Negative regulation of Erk1/2 cascade	6.69
	Adrenomedulin signalling	1.85	Cell death	7.15	Endothelial cell differentiation	5.98
	Focal adhesion assembly	1.75	Response to oxidative stress	5.91	Ossification	4.74
	Adherens junction organisation	1.67	Response to TGF-β	5.02	Response to TGF-β	4.70
	Calcitonin family receptor signalling pathway	1.61	Mesenchyme development	4.11	EC fate commitment	3.33
			Collagen biosynthesis	3.68	Endocardial cushion	3.31
	IGFR like signalling pathway	1.42	Vascular permeablity	2.75	Collagen biosynthesis	3.26
	EC development	1.38	Endocardial cushion	2.69	Negative regulation of nitric oxide biosynthesis	3.21
	Establishment of EC barrier	1.38	Cell aging	2.64	Mesenchyme morphogenesis	3.13
	Establishment of cell polarity	1.35	SMAD signalling	2.47	Inactivation of MAPK activity	2.69
Downregulated	Collagen activated TK signalling	2.87	Apelin receptor signalling	2.02	Cell communication	5.95
	Apelin receptor signalling	2.32	Activin receptor signalling	1.68	Cellular Homeostasis	4.81
	Cell aging	2.49	TNF secretion	1.55	Homeostasis of number of cells	4.55
	Cellular senescence	2.11	IFN-a production	1.53	Heart morphogenesis	4.38
	Negative regulation of angiogenesis	1.77	Vasculature development	7.99	Response to BMP stimulus	4.06
			Cell adhesion	5.00	Negative regulation of sprouting angiogenesis	3.49
	Cell migration in endocardial cushion formation	1.72	Cell number maintenance	4.05	Vasculature development	3.42
			EC proliferation	3.66	Phosphotidylinositol signalling	3.08
	Condensed mesenchymal cell proliferation	1.72	VEGF activated PDGFR pathway	2.38	Positive regulation of nitric oxide signal transduction	3.04
	TGF-β1 Production	1.54	Lipid homeostasis	1.80		
	Membrane permeablity	1.42	Extracellular matrix assembly	1.61		

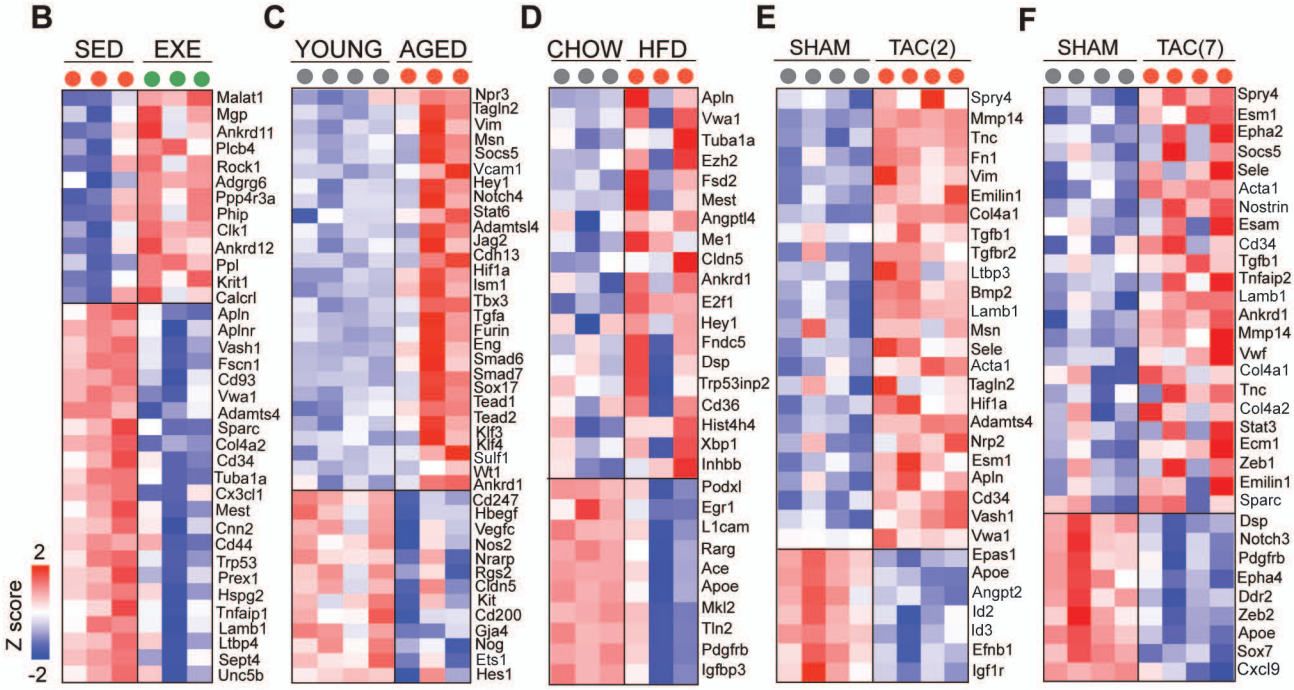

Figure 3. Cardiovascular disease risk factors activate mesenchymal gene program in cardiac EC. A. Gene ontology analysis of up- and downregulated genes. Note the opposite changes by exercise training compared to the CVD risk factors. **B-F.** Heatmaps showing the differential gene expression of endothelial and mesenchymal genes associated to endothelial-to-mesenchymal transition (EndMT). Genes are selected based on the previously published datasets (references are found in the supplementary table 5A-E). In the figure panel A-F, the up- and downregulated genes with the FDR (Benjamini-Hochberg adjusted pvalue) threshold of 0.05 were considered. In the heartmap, each color coded circles (Red, Green and Black) indicate the gene expression data obtained from individual biological sample per experimental group. N=3-4 mice/group.

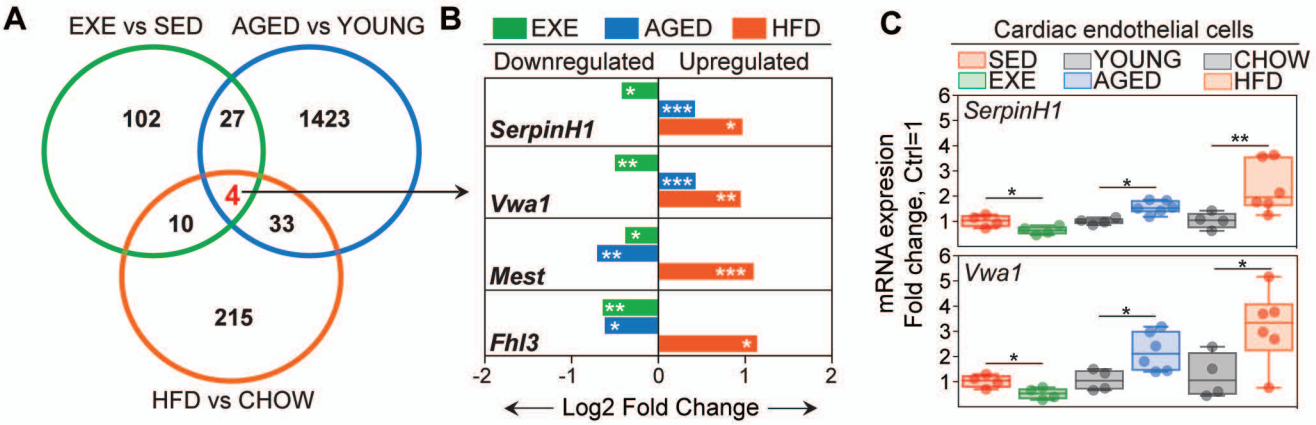

D

Uniprot ID	Gene	Subcellular Localisation	SignalP 4.0	TMHMM	TargetP 2.0	SecretomeP 1.0
P19324	*SerpinH1*	ER (lumen)	Signal peptide	-	SP	Secreted
Q8R2Z5	*Vwa1*	Extracellular space	Signal peptide	-	SP	Secreted
Q07646	*Mest*	ER (membrane)	-	-	SP	Secreted
Q9R059	*Fhl3*	Nucleus	-	-	-	-

SignalP 4.0, Predicts the presence and location of signal peptide cleavage site; TMHMM, Transmembrane helix prediction; TargetP2.0, Predicts the presence of signal peptide; SecretomeP1.0, predicts the presence of non-classical protein secretion.

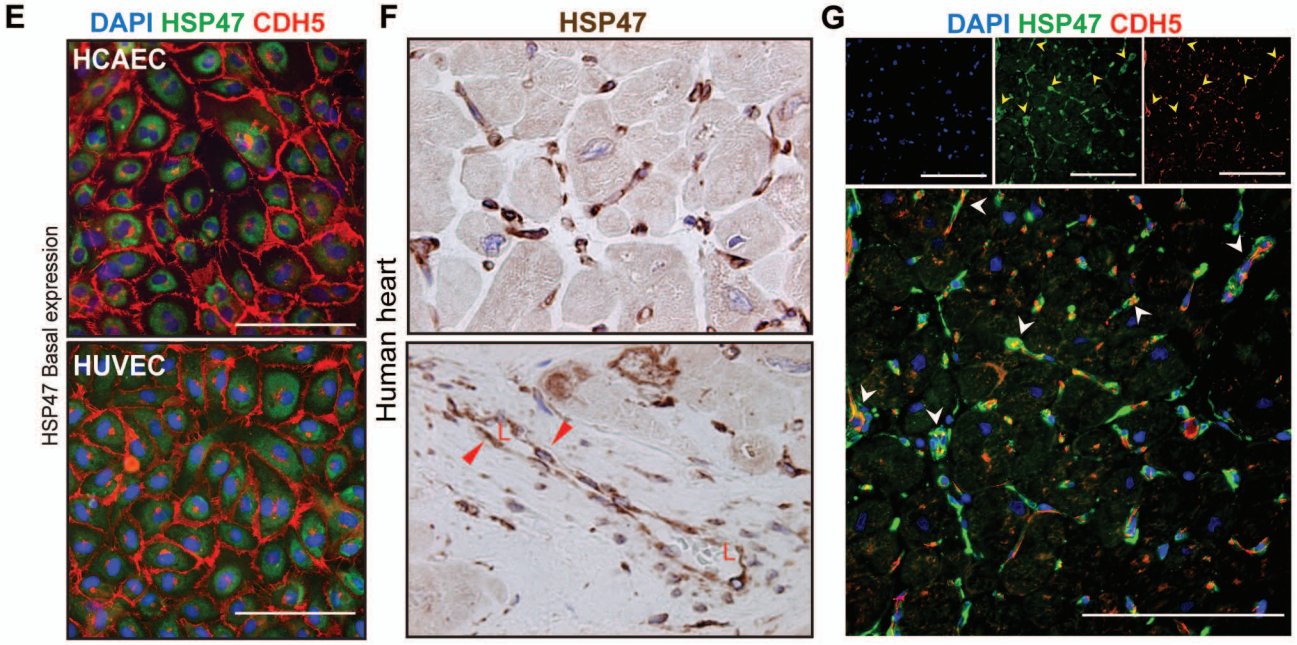

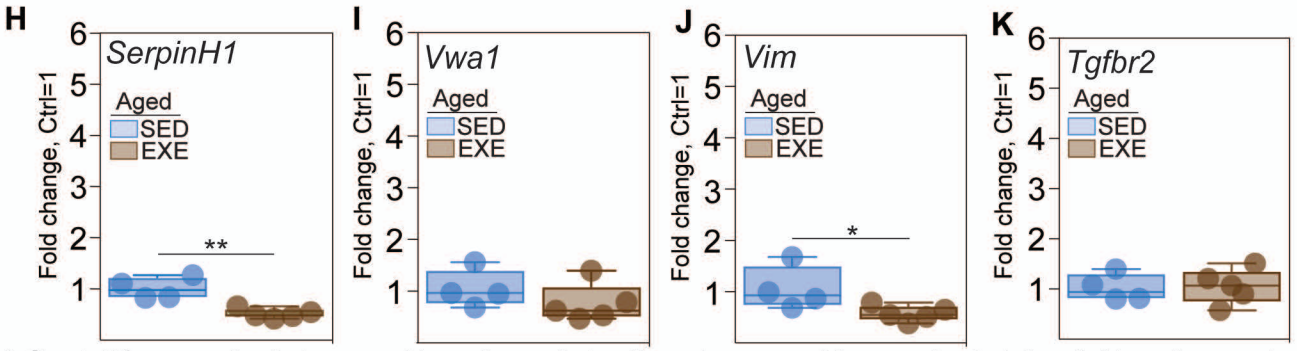

Figure 4. SerpinH1 expression is increased by aging and obesity and repressed by exercise training. A. Venn diagram showing the overlap of differentially expressed genes between the experiments. Four genes were identified to be significantly affected by aging, obesity and exercise (SerpinH1, Vwa1, Mest and Fhl3). **B.** Bar plot showing the expression pattern of these four genes. In panel **A** and **B**, the up- and downregulated genes with the FDR (Benjamini-Hochberg adjusted p-value) threshold of 0.05 were considered to be significant (N=3-4 mice/group). **C.** qPCR Validation of SerpinH1 and Vwa1 normalized to HPRT1 (N=4-6 mice/group). **D.** In silico secretome analysis of the identified genes. **E-G.** Representative immunofluorescent and immunohistochemistry images showing the expression of SERPINH1 /HSP47 in human EC and human heart samples (red arrow head in the bottom panel F indicates the expression in large vessels and "L" indicate vessel lumen. White arrowheads in the panel G denote the co-expression of HSP47 and CDH5 in coronary vessels (yellow signal). **H-K.** mRNA expression of SerpinH1, Vwa1, Vim and Tgfbr2 in the cardiac ECs of sedentary and exercise trained aged mice (N=4-5/group). Scale bar 100 µm. Data is presented as mean ± SEM. Student's t test was used, *p<0.05, **p<0.01, ***p<0.001.

Figure 5

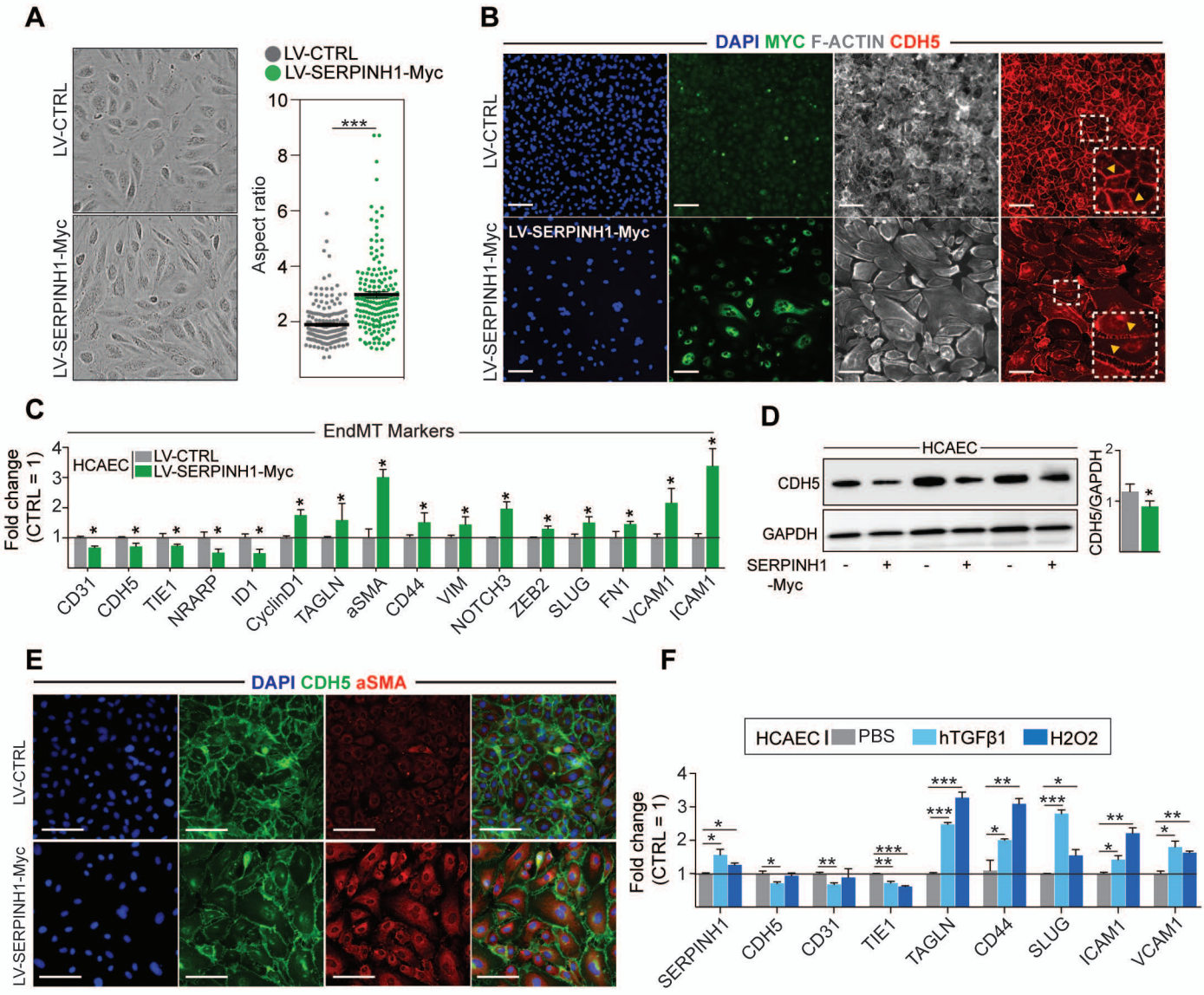

Figure 5. Overexpression of SERPINH1 modifies the EC phenotype and induces mesenchymal gene expression in human cardiac ECs. A. Representative phase contrast images of live human cardiac arterial EC (HCAEC) transduced with LV-CTRL and LV-SERPINH1-Myc and quantification of the aspect ratio (length to width ratio) of the cell. **B.** Representative immunofluorescent images showing the expression of Myc-tagged SERPINH1 in green, F-Actin in grey and CDH5/VE-Cadherin in red. The insert within the white box shows magnified view of VE-Cadherin junctions in HCAECs. **C.** qPCR analysis of endothelial and mesenchymal markers in SERPINH1 overexpressing cells. **D.** Western blot analysis and quantification of CDH5/VE-cadherin expression in the SERPINH1 overexpressing HCAECs (normalized to GAPDH). **E.** Representative immunofluorescent images showing DAPI in blue, CDH5/VE-Cadherin in green and a-smooth muscle actin (aSMA) in red. **F.** qPCR analysis of SERPINH1 and EndMT markers in HCAECs stimulated with TGF-β1 (50ng/ml) or H2O2 for five days. In panel **A, C, D** and **F**, N=3 biological replicates/group were analysed. Scale bar 100 μm. Data is presented as mean ± SEM. Student's t test was used, *p<0.05, **p<0.01, ***p<0.001.

Figure 6

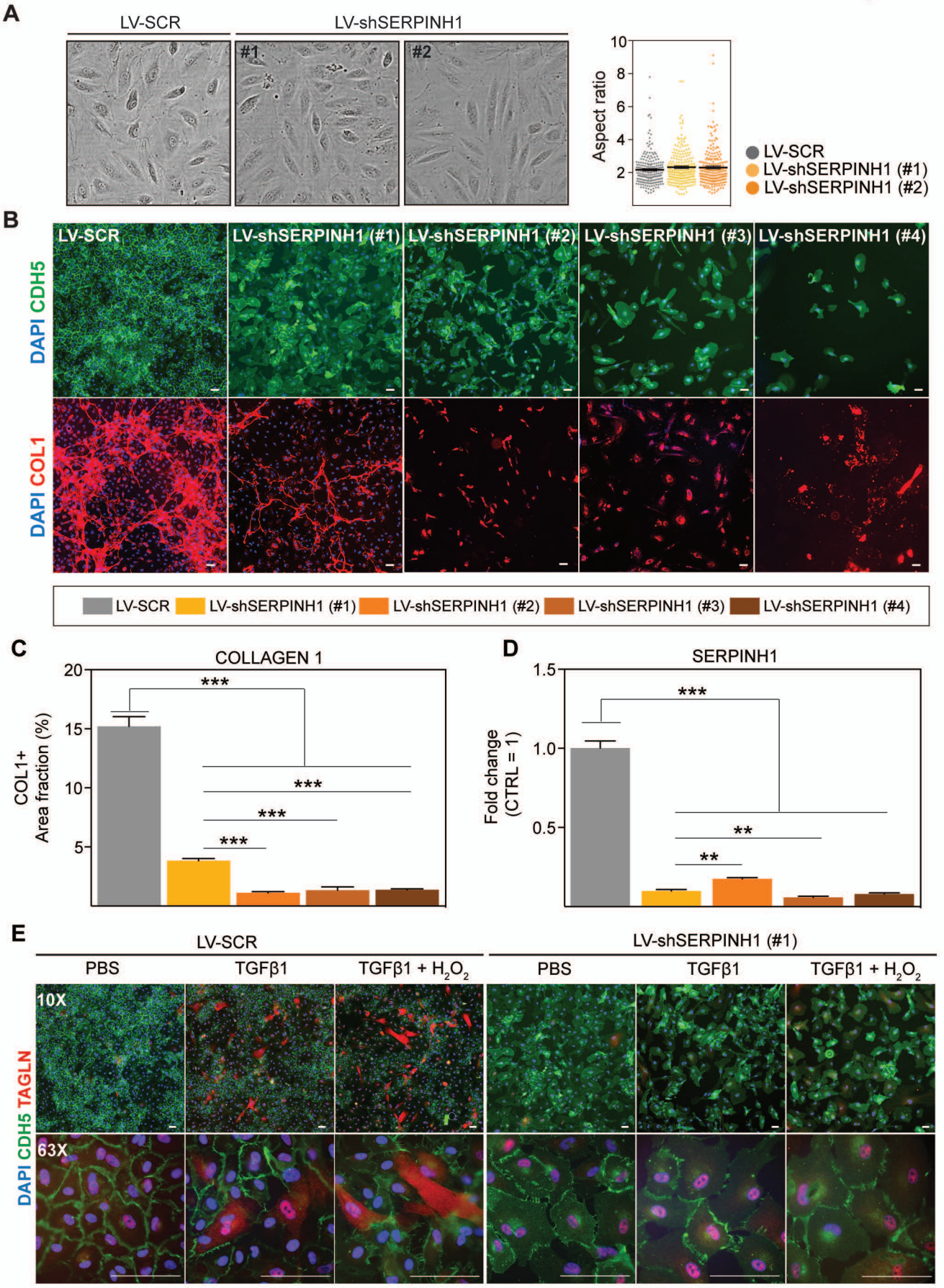

Figure 6. SERPINH1/HSP47 silencing in human cardiac EC inhibits collagen production and secretion. A. Representative phase contrast images of live HCAECs transduced with LV-SCR and LV-shSERPINH1 (#1 and #2) and quantification of the aspect ratio (length to width ratio) of the cells after two days of silencing. **B.** Representative CDH5/VE-Cadherin immunofluorescent images (green) showing the cell morphology and density after ten days of SERPINH1 silencing. Collagen 1 staining is shown in red, and quantification of Collagen 1 is shown in **C. D.** qPCR analysis of SERPINH1 deletion levels using four independent constructs. **E.** Representative immunofluorescent images showing TAGLN expression in the control and SERPINH1 silenced HCAECs treated with recombinant human TGF-b1 with and without H2O2 for five days. In panel **A, C and D**, N=3 biological replicates/group were analysed. Scale bar 100μm. Data is presented as mean ± SEM. Student's t test was used, *p<0.05, **p<0.01, ***p<0.001.

Figure 7

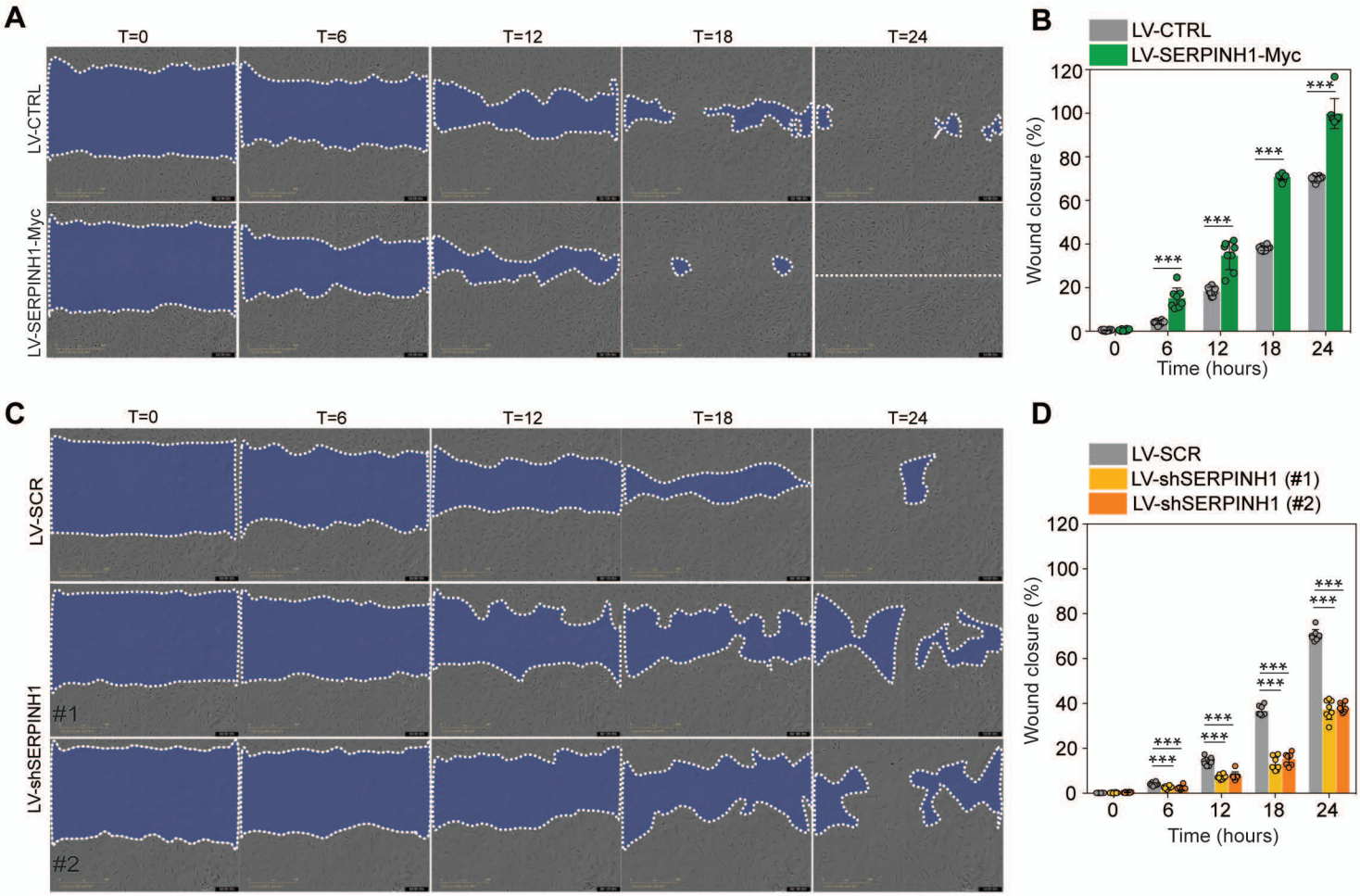

Figure 7. SERPINH1 overexpression enhances and silencing inhibits wound closure in vitro. A-B. Representative phase contrast images of scratch wound healing assay performed in HCAECs treated with LV-CTRL and LV-SERPINH1, and quantification 1 of the wound closure (%) with respect to time (hours). **C-D.** Representative phase contrast images of scratch wound healing assay performed in HCAECs treated with LV-SCR and LV-shSERPINH1 (#1 and #2), and quantification of the wound closure (%) with respect to time (hours). In the panel A and C, the blue area within the white dotted region indicate the wound area. In panel **B and D**, N=8 biological replicates/group were analysed. Data is presented as mean ± SEM. Student's t test was used, *p<0.05, **p<0.01, ***p<0.001.

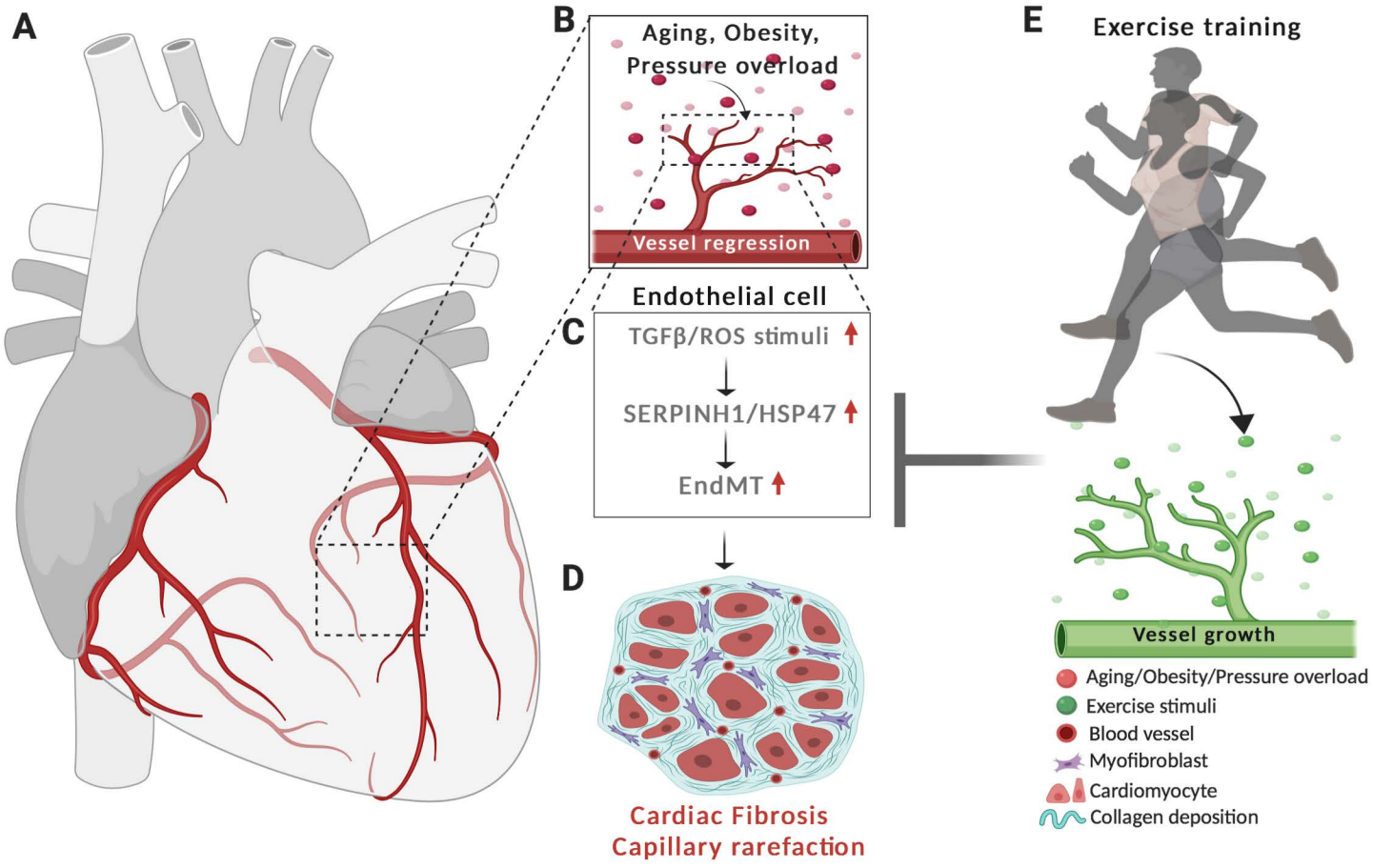

Graphical Abstract of the cardiovascular disease risk factor mediated activation of TGF- β signaling and acquisition of mesenchymal gene features in cardiac EC . CVD risk factors aging, obesity and pressure overload trigger the regression of coronary vasculature by activating TGF-β/ROS signaling pathways to induce the expression of SerpinH1/Hsp47 and gains mesenchymal gene signature. SerpinH1/Hsp47 and EndMT are both involved in the development of tissue fibrosis by increasing collagen deposition in extracellular matrix. Exercise training, in turn, increased the coronary vasculature density and EC number and repressed TGF- β and senescence related pathways.

Supplementary Material

Cardiovascular disease risk factors induce mesenchymal features and senescence in cardiac endothelial cells

Karthik Amudhala Hemanthakumar [1,2], Fang Shentong [1,3], Andrey Anisimov [1,3], Mikko I Mäyränpää [4], Eero Mervaala [5], Riikka Kivelä [1,2]

[1]Wihuri Research Institute, Helsinki, Finland

[2]Stem cells and Metabolism Research Program, Research Programs Unit, Faculty of Medicine, University of Helsinki, Helsinki, Finland

[3]Translational Cancer Medicine Research Program, Research Programs Unit, Faculty of Medicine, University of Helsinki, Helsinki, Finland

[4]Pathology, Helsinki University and Helsinki University Hospital, Helsinki, Finland

[5]Department of Pharmacology, Faculty of Medicine, University of Helsinki, Helsinki, Finland

Address for correspondence:

Dr. Riikka Kivelä, PhD

Stem cells and Metabolism Research Program

Research programs unit, Faculty of Medicine

University of Helsinki, PO Box 63, 00014 Helsinki, Finland

Tel: +358 2941 25516

Email: riikka.kivela@helsinki.fi

Materials and Methods

Mouse Models

All animal experiments were approved by the committee appointed by the District of Southern Finland. Male C57BL/6J 7-8 -week adult wild type mice were purchased from Janvier Labs and used in the following experimental set-ups: physical activity (progressive exercise training vs sedentary), obesity (high-fat fed for 14 weeks vs chow), aging (18 months vs 2 months) and pressure overload/heart failure (transaortic constriction for two- and seven-weeks vs sham). Female C57BL/6J wild type mice of 19-24 months old were used for a separate exercise training experiment. The mice were housed in individually ventilated cages and acclimatized at least for one week in the animal facility before any experiments. The cohort size (n) for each experiment is indicated in the figures or figure legends.

Exercise Training

Ten-week-old C57BL/6J male mice or 19 to 24 months old female mice were trained on a treadmill (LE 8710, Bioseb). The mice were familiarized to the treadmill for three consecutive days with low speed (8-10 cm/s). Progressive training program consisted of 1-1.5 h training bouts five days a week for a total of six weeks with increasing speed, incline and/or duration each week. The following parameters in the treadmill controller were opted, tread inclination: 0°-10°; minimum and maximum tread speed: 10cm to 30cm per second; shock grid intensity: 0.2 mA. The aged mice were exercise-trained for four weeks and the same procedures were followed during the training program.

High Fat feeding

Ten-week-old C57BL/6J male mice were fed with standard chow diet or high-fat diet (HFD) containing 60% kcal derived from fat (Research Diets, D12492) for 4 or 14 weeks and used for immunohistochemistry or RNA-seq analysis, respectively.

Transverse Aortic Constriction Surgery

Ten-week-old C57BL/6J male mice were anesthetized with ketamine and xylazine. The mice were placed in supine position and intubated. The skin along the supra-sternal notch to mid sternum was incised to perform sternotomy to expose the aortic arch, right innominate and left common carotid arteries together with the trachea. Ligation of the transverse aorta between the right innominate left common carotid arteries against blunted 27-gauge needle with a 7-0 suture was performed and the needle was gently removed. The sternum and skin were ligated with monofilament polypropylene suture. Mice were placed in a warm chamber to recover, treated with analgesics (0.05mg/kg of Temgesic i.m.) at the time of the surgery and twice a day for following two days. For the control group (sham), all the steps in the surgical procedure were followed, except constricting the aorta. One group was killed two weeks and another group seven weeks after the surgery. Echocardiography was performed once a week during the experiment.

Echocardiography

To analyze cardiac function and ventricle dimensions, two-dimensional echocardiography images were acquired (Vevo 2100 Ultrasound, FUJIFILM Visual Sonics). The left ventricular internal diameter, left ventricular posterior wall thickness, interventricular septum thickness at end-systole and end-diastole were measured in M-mode along the parasternal short axis view, and analyzed by Simpson's modified method [1].

Body Fat Measurement

The mice were anesthetized with ketamine and xylazine and the percentage of total body fat was measured using dual energy x-ray absorptiometry (Lunar PIXImus, GE Medical systems).

Oral Glucose Tolerance Test

Mice were fasted for four to five hours before the experiment. Glucose (1g/kg) was administered by oral gavage to mice. Blood from the tail tip was used to measure glucose levels at the following time points (15, 30, 60 and 90 min) using blood glucose meter (Contour, Bayer).

Immunofluorescent Staining

Frozen mouse heart sections (10μm) were cut with cryomicrotome and stained as described previously [1]. The primary antibodies are listed in the **Supplementary Table 2**. Primary antibodies were detected with Alexa 488, 594 or 647 -conjugated secondary antibodies (Molecular Probes, Invitrogen). The sections were mounted with Vectashield Hard Set mounting media with DAPI (Vector Laboratories). The images were acquired with 20X, 40X air or 40x oil immersion objectives using AxioImager epifluorescent microscope (Carl Zeiss). The stained micrographs were initially adjusted for threshold, and an area fraction tool was used to quantify the area percentage of the vessels and collagen (Image J software, NIH).

Human Heart samples

Human heart samples were obtained from 4 organ donor hearts, which could not be used for transplantation e.g. due to size or tissue-type mismatch. The collection was approved by institutional ethics committee and The National Authority for Medicolegal Affairs.

Immunohistochemistry

The human paraffin heart sections (4µm) were cut, deparaffinized and rehydrated with xylene, descending concentration series of ethanol (99%, 95%, 70% and 50%) and H_2O, and incubated in high pH antigen retrieval buffer containing 10 mM Tris, 1 mM EDTA, 0.05 % Tween 20 (pH 9.0). For HSP47 immunohistochemical analysis, VECTASTAIN Elite ABC kit (PK-6100) and DAB substrate was used to label and amplify the antibody signal. The 20X or 63X images were acquired with light microscope (Leica). For immunofluorescent staining, after the antigen retrieval step the sections were blocked with donkey immunomix (5% normal donkey serum, 0.2% BSA, 0.3% Triton X-100 in PBS), incubated overnight at 4°C with the primary antibodies for HSP47 and VE-Cadherin (CDH5) and detected with Alexa 488 and 594 conjugated secondary antibodies (Molecular probes, Invitrogen). The sections were mounted with Vectashield hardset with DAPI (Vector labs) and 40X images were acquired using AxioImager epifluorescent microscope (Carl Zeiss).

Isolation of Cardiac Endothelial Cells

The harvested hearts were briefly rinsed in ice-cold Dulbecco's phosphate-buffered saline (DPBS, #14190-094, Gibco) supplemented with 0.3mM calcium chloride ($CaCl_2$), cut opened longitudinally into two halves to expose the cardiac chambers and minced longitudinally and transversly into small pieces. To enzymatically dissociate the heart, 4ml of pre-warmed digestion media (1mg/ml of each collagenase types (type I (#17100-017), type II (#17101-015) and type IV (#17104-019) from Gibco were dissolved in DPBS containing 0.3mM $CaCl_2$) and added to the minced hearts, incubated in water bath at 37°C for 25 min. During the digestion process, the samples were very gently mixed by vortexing for every 5 min. After incubation, the cell suspension was gently passed through T10 serological pipette 20 times. To neutralize the digestion, 10ml of rinsing media (Dulbecco's modified eagle medium (#31053-028) supplemented with 10% heat inactivated FCS) was

added to the cell suspension and filtered through the 70µm nylon cell strainer (Corning, #352350). Throughout the isolation process the cell suspensions were centrifuged for 5min, 300g and 4°C between each rinsing step. The cell pellet was resuspended in 5ml of ice-cold staining buffer (DPBS containing 2% heat inactivated FCS and 1mM EDTA). Before antibody staining, the cells were incubated with Fc receptor blocking antibody (CD16/32) for five minutes. The cells were incubated with the CD31, PDGFRa/CD140a, CD45, and Ter119 antibodies for 30 min **(Supplementary Table 2 for the antibody details)**. Prior to fluorescent associated cell sorting (FACS), the cells were rinsed twice with the staining buffer and filtered through 5ml cell strainer tubes (Corning, #352235).

Fluorescent Associated Cell Sorting (FACS)

The cells were passed through a 100µm nozzle. Multiple light scattering parameters for forward- and side-scatter properties of the cells were employed to gate, analyze and sort live cardiac endothelial cells. Initially, total cells were gated based on the forward and side-scatter area of the cells (FSC-A and SSC-A). The single cells were selected depending on forward scatter parameters area, height and width of the cells (FSC-A, FSC-H or FSC-W). DAPI was used to determine live and dead cells. To enrich and FACS sort pure and viable cardiac ECs, endothelial cells were stained with CD31, mesenchymal cells with PDGFRa/CD140a, leucocytes with CD45 and red blood cells with Ter119. The live cardiac endothelial cells were defined as $CD31^{+}$ $CD45^{-}$ $Ter119^{-}$ $CD140a^{-}$ $DAPI^{-}$. Cells were sorted using FACS Aria II (BD Biosciences), the data was acquired with BD FACSDIVA v8.0.1 and further analyzed with FlowJo v10.1 (FlowJo, LLC) software. We verified the enrichment and purity of the FACS sorted Cardiac EC population (CD31+ PDGFRa (CD140a)- CD45- Ter119- DAPI-) by QPCR analysis for classical cardiac EC markers. Recently, we have used the same isolation method for single-cell RNAseq experiments, and these results show that

there is about 3% contamination from other cells types, mainly pericytes and hemangioblasts.

RNA isolation

The sorted cardiac endothelial cells were immediately suspended in lysis buffer (350µl of RLT buffer plus 10µl of β-mercaptoethanol), the cells were homogenized in QIAshredder (#79654, Qiagen) and the RNA was purified using RNeasy Plus Micro Kit (#74034, Qiagen) according to the manufacturer's instruction. The RNA integrity was analyzed with bioanalyzer (Agilent Tape Station 4200) and the concentration was determined by Qubit fluorescence assay (ThermoFisher). The cells from the post sort fractions were stained with propidium iodide (PI) and the viability of the cells were determined by Luna automated cell counter. The purity of the post sort fraction was determined by QPCR analysis for endothelial cell markers.

RNA sequencing of cardiac EC

Indexed cDNA library was synthesized using SMARTer Stranded Total RNA-Seq Kit V2 – Pico Input Mammalian (Takara Bio, USA) kit according to the manufacturer's instructions. The library quality was determined using bioanalyzer, and sequenced using illumina NextSeq 550 System with the following specifications: 1 X 75bp, 50M single end reads were sequenced using NextSeq 500/550 High-Output v2.5 kit.

Differential gene expression

The sequenced reads were analyzed with the following software packages embedded in the Chipster analysis platform [2] (v3.12.2; https://chipster.csc.fi). Trimmomatic tool [3] (https://chipster.csc.fi/manual/trimmomatic.html) was used to preprocess Illumina single end

reads. The HISAT2 package [4] (https://chipster.csc.fi/manual/hisat2.html) was employed to align the reads to mouse genome GRCm38.90 and the HTSeq count tool [5] (https://chipster.csc.fi/manual/htseq-count.html) to quantify the aligned reads per gene. The raw read count table for genes generated utilizing the HTSeq count were used as an input to perform two-dimensional principal component analysis (PCA) and unsupervised hierarchical clustering analysis using DESeq2 Bioconductor package [6] (https://chipster.csc.fi/manual/deseq2-pca-heatmap.html). Next, to perform the differential gene expression (DGE) analysis, the DESeq2 Bioconductor package [6] was used. The advantage of DEseq2 tool is sensitive and precise for analyzing the DEG in studies with few biological replicates. To reliably estimate the within group variance, Empirical Bayes shrinkage for dispersion estimation was used and a dispersion value for each gene was estimated through a model fit procedure (refer to the **Figure S5A**, which illustrates the shrinkage estimation for the experimental conditions). The gene features obtained after the dispersion estimation were used to perform statistical testing. Next, negative binomial generalized linear model was fitted for each gene and Wald test (raw p-value) was calculated to test the significance. Finally, DEseq2 applies Benjamini-Hochberg correction test to control the false discovery rate, FDR (refer to the **Figure S5B** indicating the distribution of raw and FDR adjusted pvalue for the experimental conditions). In our DEG analysis, we have set the FDR (p adj.) cut-off as less than or equal to 0.05 (FDR/p-adj ≤ 0.05) for pathway analysis and gene overlap analysis. The RNA sequencing data is deposited in the GEO database, under the series accession number **GSE145263**.

Gene Function and Pathway Analysis

The gene function and pathway analysis of the DGE were determined by performing statistical overrepresentation test using the PANTHER classification system [7] (V.14.1;

http://www.pantherdb.org). The p<0.05 was considered for the further analysis and the data is presented as -log2(pvalue).

Gene Overlap and *in silico* Gene Characterization

The differentially expressed up- and downregulated genes (adjusted P-value 0.05) from the different experimental conditions were imported to VENNY 2.1 venn-diagram analysis software (BioinfoGP; https://bioinfogp.cnb.csic.es/tools/venny/) to identify genes which were significantly affected by several experimental conditions. The MetazSecKB knowledgebase [8] (http://proteomics.ysu.edu/secretomes/animal/index.php), TargetP2.0 server [9] (http://www.cbs.dtu.dk/services/TargetP/index.php) and SecretomeP1.0 server [10] (http://www.cbs.dtu.dk/services/SecretomeP-1.0/) were used to characterize molecular functions, subcellular localizations and possible secretion properties of the identified common genes.

Cell Culture and Lentiviral Production

Human umbilical vein endothelial cells (HUVEC) and human cardiac arterial endothelial cells (HCAEC) were purchased from PromoCell. Both HUVEC and HCAEC were cultured and maintained in endothelial cell growth Basal Medium MV (C-22220, PromoCell) supplemented with Supplement Pack GM MV (C-39220, PromoCell) and gentamycin. For both gene overexpression and silencing studies, 80% confluent monolayer culture of HUVECs and HCAECs were used.

To overexpress SERPINH1 in EC, we cloned a lentiviral vector FUW-hSERPIH1-Myc (map and plasmid available by request). A scrambled sequence in the same vector was used as a control. 293FT cells (ATCC) were cultured and maintained in DMEM supplemented with

10% FCS and L-glutamine, and co-transfected with the lentiviral packaging plasmid vectors CMVg, CMV$_{\Delta}$8.9 and the target plasmid. The supernatants were collected at 48- and 72-hours, and concentrated by ultracentrifugation as described previously [11]. For overexpression, HUVEC and HCAEC were transfected with lentivectors for 48 hours. For gene silencing studies, HCAEC were treated with lentivectors encoding for four independent clones of human shSERPINH1 for 24h. Subsequently, the cells were treated with puromycin (2ug/mL) for 48 hours to select the transduced cells. After selection, the cells were used for further analysis. The clone id and target sequence for human shSERPINH1 constructs are shown in the **Supplementary Table 3**.

Scratch wound assay

The SERPINH1 overexpressed or silenced HCAECs were seeded in the IncuCyte ImageLock 96-well microplate precoated with 0.1% gelatin and cultured in complete EC growth medium. To the confluent cell monolayers, 700 – 800 micron scratch wounds were introduced with IncuCyte WoundMaker, the wells were briefly rinsed with and maintained in complete EC growth medium. The kinetics of the cell migration were recorded and 10X phase contrast time-lapse images were acquired using IncuCyte Live-Cell Analysis System. The wound closure region was measured by Edge-detection and thresholding method in Image J software (NIH). The data is presented is as wound closure (%) relative to time.

EndMT assay

The coverslips or six well plates were precoated with 0.1% gelatin for 20min at 37°C, scrambled or SERPINH1 silenced HCAEC were seeded and cultured in complete EC growth medium. The cells were treated with or without 50ng/ml of recombinant human TGF- β (R&D

Technologies) and/or 200μM hydrogen peroxide (Acros organics) for five days as described previously [12, 13].

Cell Staining

The cells grown on the coverslips were fixed with 4% PFA in PBS for 15 min. Blocking was done using donkey immunomix and the cells were stained with primary antibodies and secondary antibodies as indicated in the Supplemental Table 2. DAPI was used to stain the nucleus, and the cells were mounted using Vectashield (Vector labs). The amount of COL1 was quantified by adjusting 10X images for threshold and area fraction tool was used to quantify the area percentage of the collagen deposition (Image J software, NIH).

Real-Time Quantitative PCR

RNA from the cultured cells was purified and isolated using NucleoSpin RNA II Kit according to the manufacturer's protocol (Macherey-Nagel). cDNA was synthesized with High-Capacity cDNA Reverse Transcription Kit (Applied biosystems, #4368814). SYBR green or TaqMan gene expression assays were performed using FastStart Universal SYBR green master mix (Sigma-Aldrich, #04913914001) and TaqMan gene expression master mix (Applied Biosystems, #4369016), respectively. mRNA expression was analyzed using Bio-Rad C1000 thermal cycler according to standardized protocol of the qPCR master mix supplier. The average of the technical triplicates for each sample was normalized to the housekeeping gene HPRT1. The mRNA expression levels were calculated and presented as fold change (Ctrl=1). The primer sequences are listed in the **Supplementary Table 4.**

Western Blotting

The cells were harvested and homogenized in lysis buffer containing 0.5%NP-40 (v/v) and 0.5%Triton X-100 (v/v) in PBS, supplemented with protease and phosphatase inhibitors (A32959, Pierce, Thermo Scientific). Protein concentration was determined using a BCA protein assay kit (Pierce, Thermo Scientific). Equal amounts of total protein were resolved in Mini-PROTEAN TGX Precast gels (Bio-Rad) and transferred to PVDF membrane (immobilon-P, Millipore). 5% BSA (wt/vol) and 0.1% Tween 20 (v/v) in TBS was used to block the membranes followed by incubation with primary antibodies **(Supplementary Table 2)** overnight at 4°C. HRP-conjugated secondary antibodies (DAKO) were used, and HRP signals were developed with Super-Signal West Pico Chemiluminescent substrate or Femto Maximum sensitivity substrate (Thermo Scientific). The blots were imaged with Odyssey imager (Li-COR Biosciences) or Chemi Doc imaging system (Bio-Rad) and quantified with Image Studio Lite Software (Li-COR Biosciences).

Statistics

The data from the individual experiments were analyzed by student's *t* test. $P<0.05$ value was considered statistically significant and P values in the graphs are shown as *$P<0.05$, **$P<0.01$ and ***$P<0.001$. The data is shown as mean ± SEM. The GraphPad Prism 7 software was used for statistical analysis.

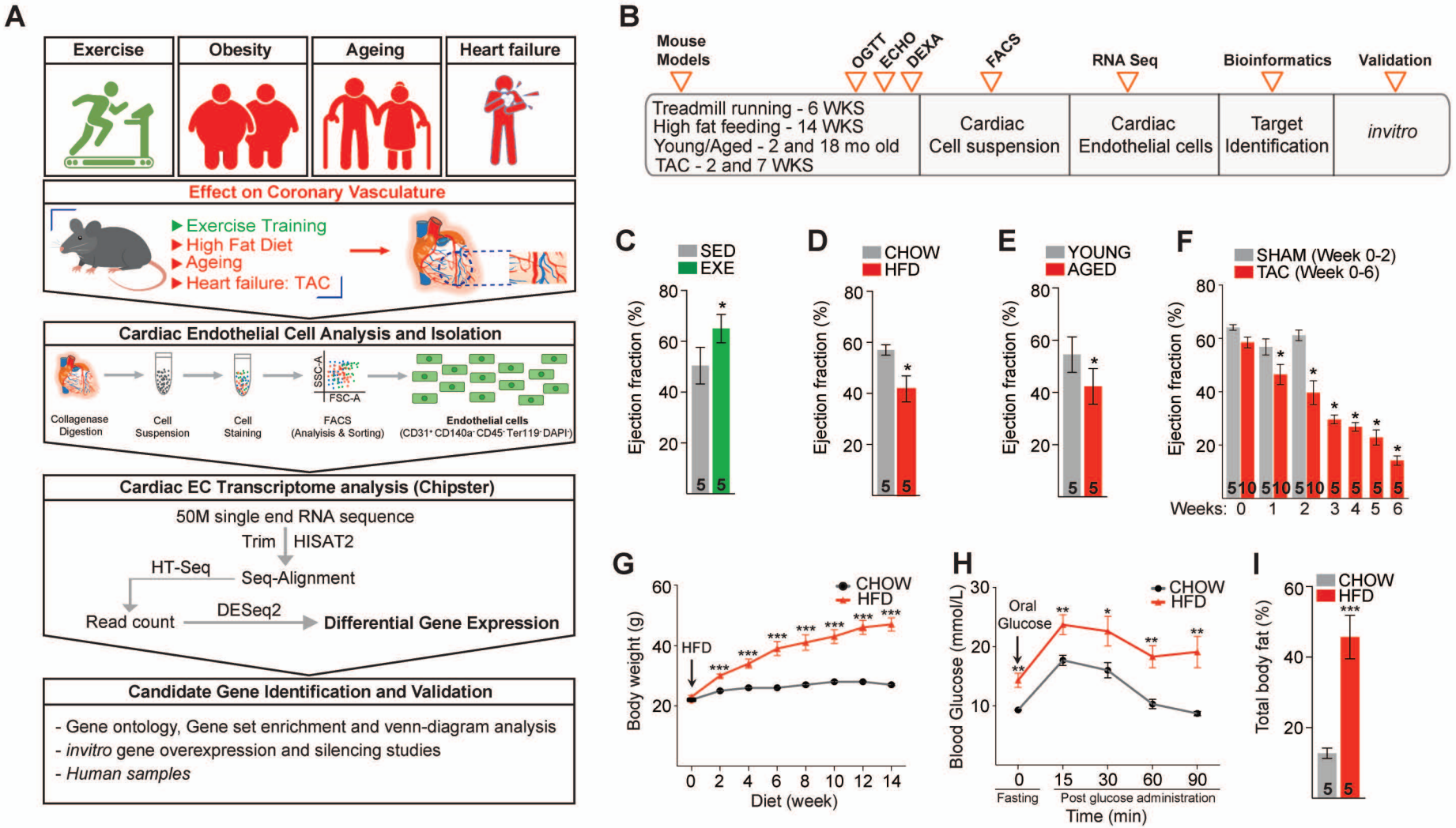

Figure S1. Schematic of the experimental set-up to elucidate the impact of cardiovascular disease risk factors on cardiac endothelial cell transcriptome and the validation of the experimental CVD risk factor models . A. Experimental workflow demonstrating the mouse models used to mimic CVD risk factors in C57Bl/6J mice, analysis and isolation of cardiac ECs by fluorescence- activated cell sorting, bioinformatic analyses of the cardiac EC transcriptome, identification and validation of candidate genes using human ECs and heart tissue. **B.** Experimental timeline of exercise training (6 weeks of treadmill running), high fat diet (14 weeks of high fat feeding), physiological ageing (18 months old) and pressure overload -induced heart failure by transaortic constriction in mice. **C-F.** Ejection fraction in each of the four experiments. **G.** Body weight (g) during the HFD experiment. **H.** Blood glucose levels during oral glucose tolerance test (mmol/L), and **I.** total body fat (%) measured after 14 weeks of high-fat diet. Data is presented as mean ± SEM. Student's t test was used, *p<0.05, **p<0.01, ***p<0.001 (In panel **C-F and I**, number of mice in each experimental group are indicated in the respective graph, In panel **G-H**, N=4-5 mice/group were analysed.

Figure S2

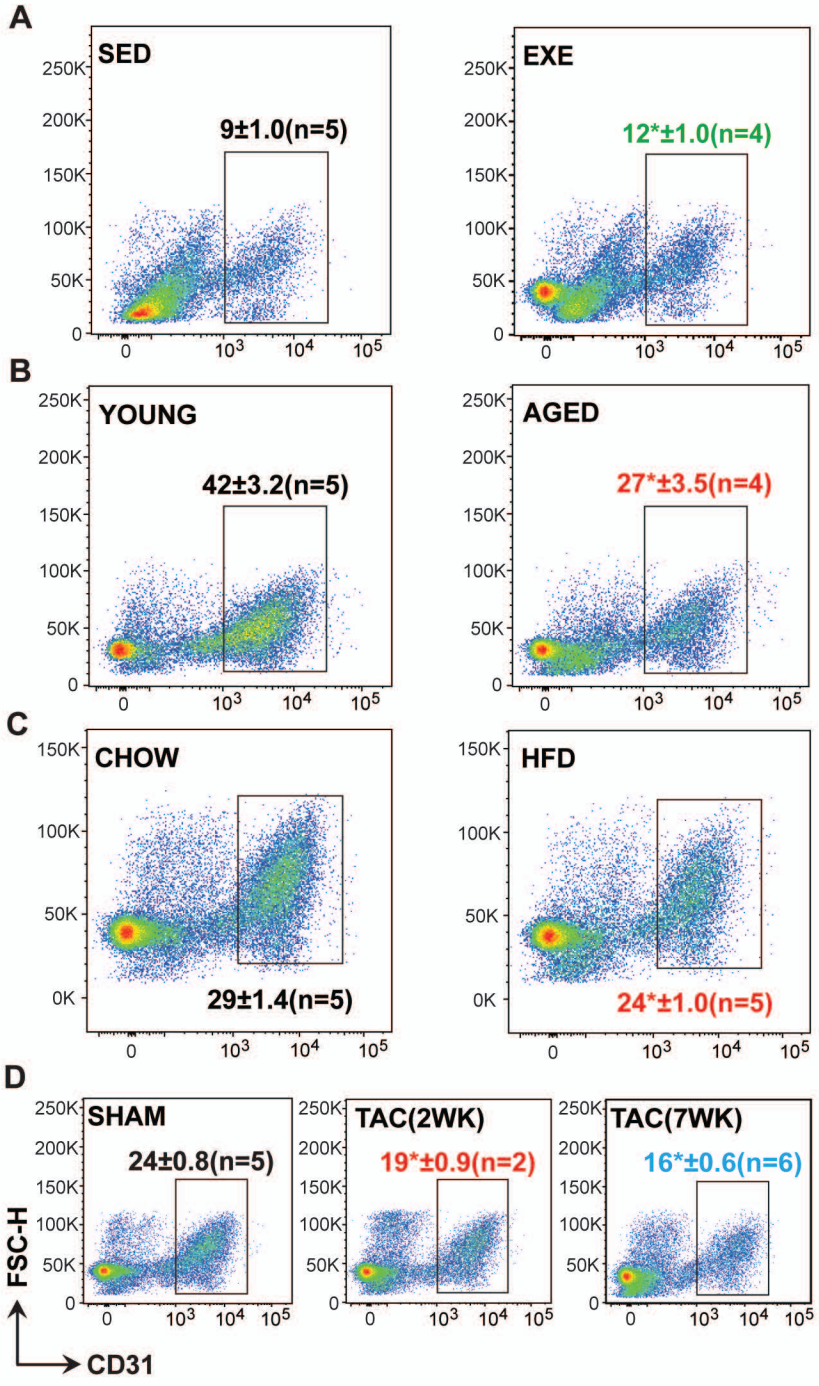

Figure S2. FACS analysis of cardiac EC. A-D. Representative pseudocolor FACS plots showing the gating and percentage of cardiac ECs (CD31+ CD140a- CD45- Ter119- DAPI-) in the different treatment groups. In panel **A-D**, number of mice in each experimental group are indicated in the respective FACS plots.

Figure S3

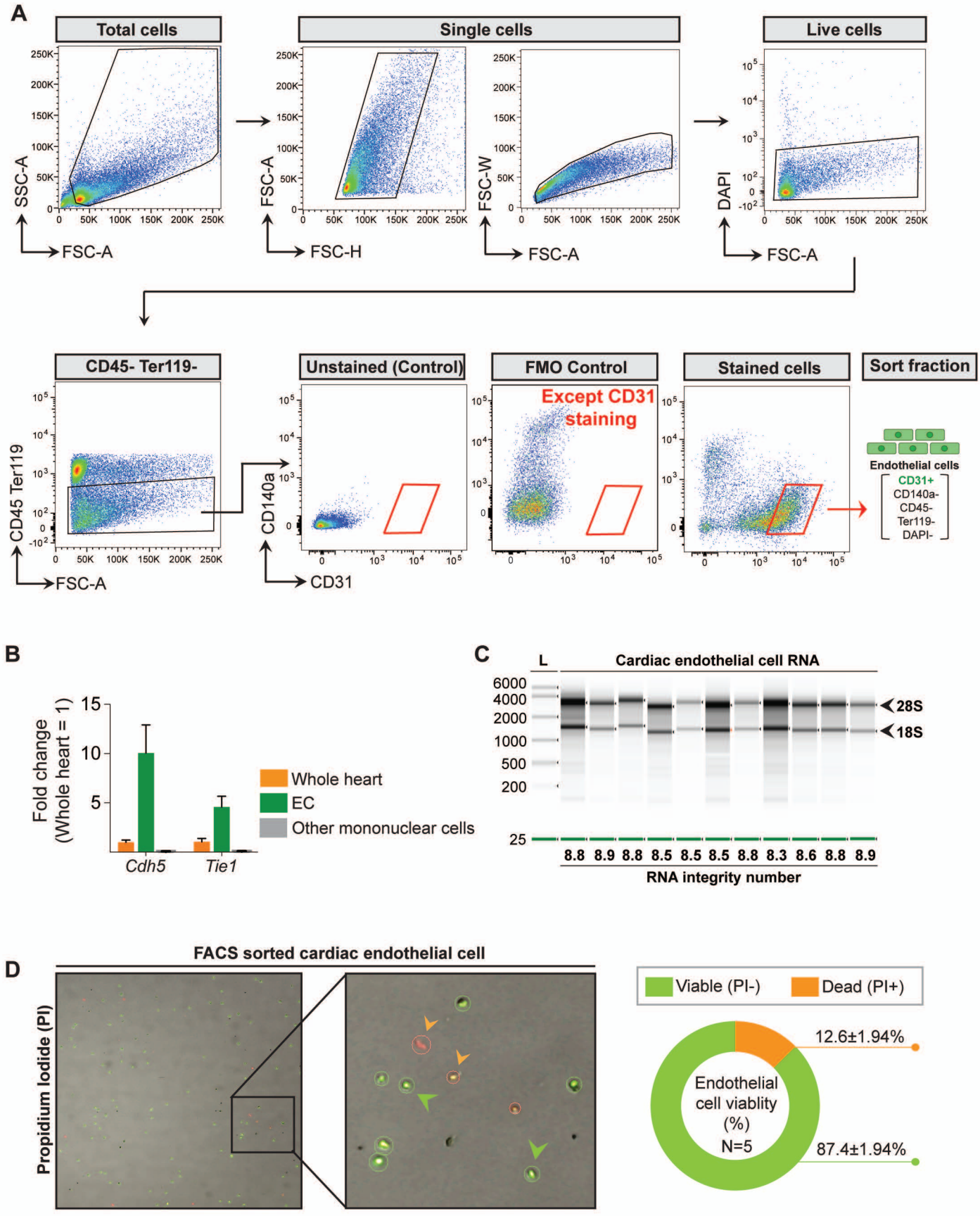

Figure S3. Quality metrics of the FACS sorted cardiac EC. A. Gating strategy to sort cardiac ECs (CD31+ CD140a- CD45- Ter119- DAPI-). **B.** Purity analysis of the post sort EC fraction by QPCR (N=4 mice/group were analyzed). **C.** Representative image of the bioanalyzer data showing the RIN values of the isolated RNA. **D.** Mononuclear cells and pie chart of the post sort EC fraction showing viable cells in green and dead cells in red.

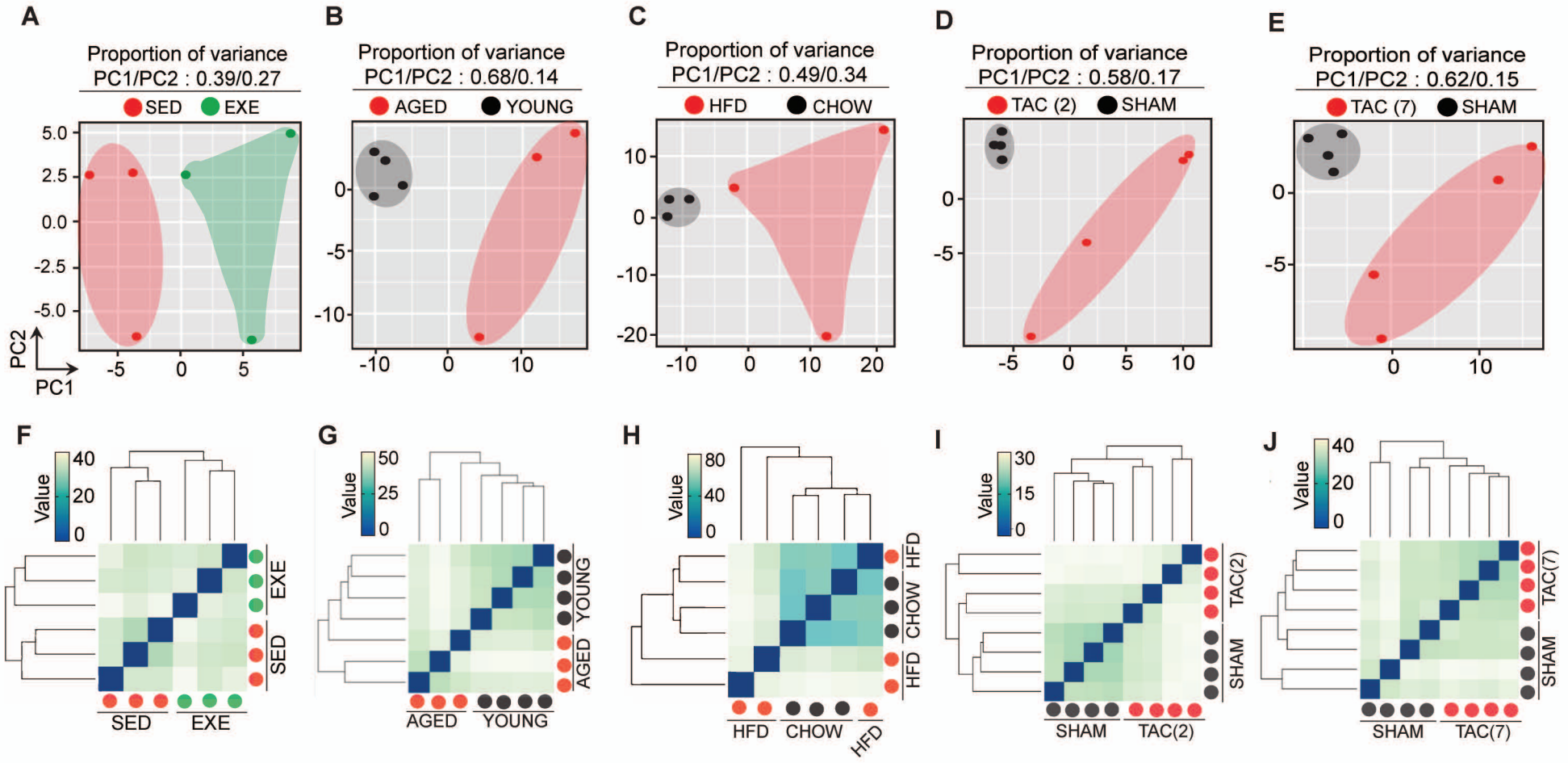

Figure S4. PCA plot and unsupervised hierarchical clustering of cardiac endothelial cell transcriptome from exercise trained, aged, obese and TAC-treated mice. A-E. Two dimensional principal component analysis, **F-J.** Unsupervised hierarchical clustering of cardiac endothelial transcriptome in the indicated experimental group. Eachcolor coded circles (Red, Green and Black) in the PCA and Unsupervised clustering plot indicate one biological sample and N=3-4 mice/experimental condition were analysed.

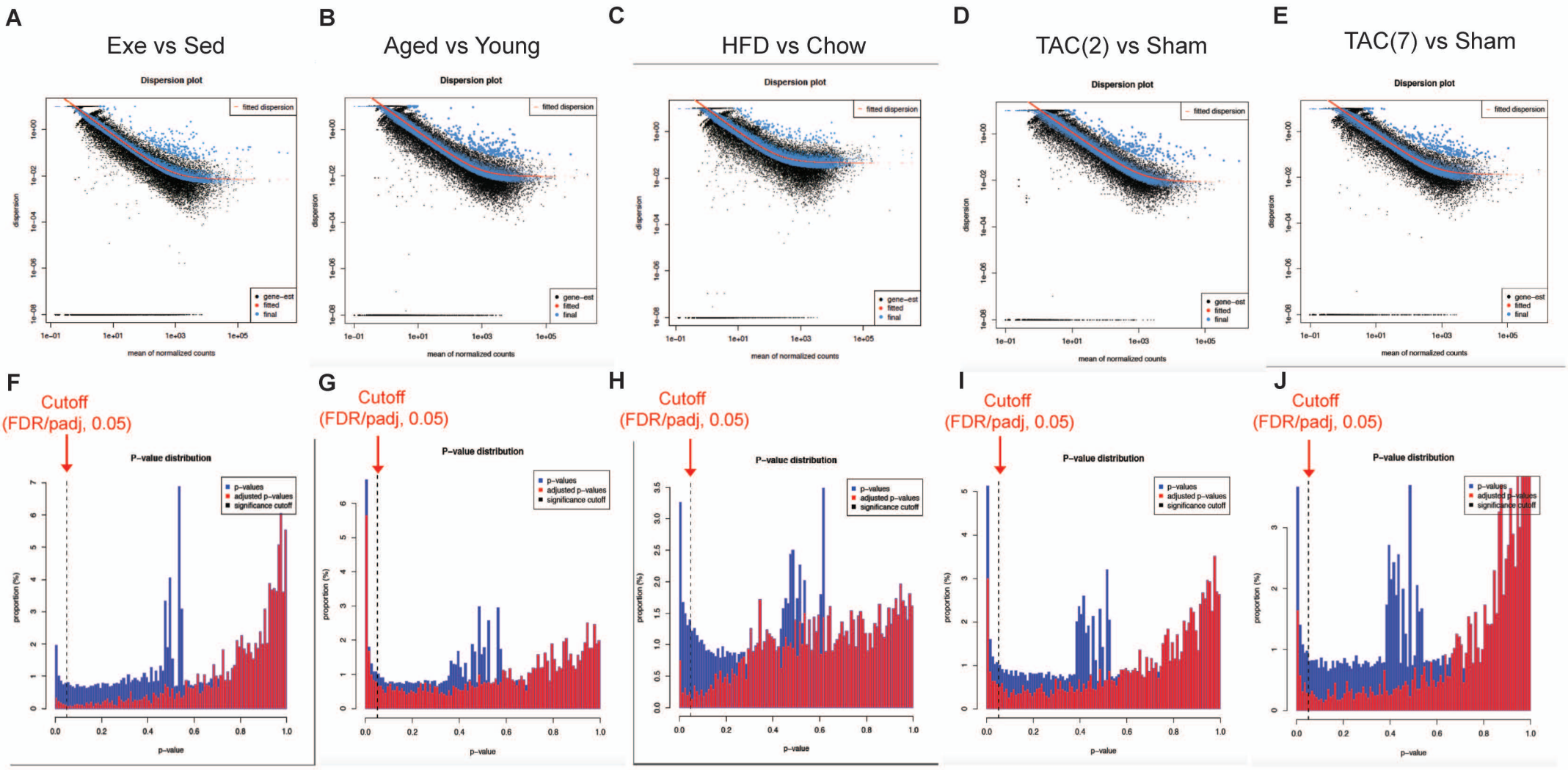

Figure S5. Dispersion mean plot and p-value distribution plot of the indicated RNA sequencing experiments. A-E. Plot of dispersion estimates at different count levels, showing black dot (Dispersion estimate for each gene as obtained by considering the information from each gene separately), Red line (Fitted estimates showing the dispersions' dependence on the mean), Blue dot (The final dispersion estimates shrunk from the gene-wise estimates towards the fitted estimates. The values are used for further statistical testing). Blue circles (Genes which have high gene-wise dispersion estimates and are hence labelled dispersion outliers and not shrunk toward the fitted trend line. **B.** Plot of the raw p-value (Wald test) indicated in blue bar and the false discovery rate distribution or adjusted p-value (Benjamini-Hochberg adjusted p-value) of the statistical test. The arrow indicates cutt-off point False discovery rate thereshold of 0.05 and the genes with FDR values less than or equal to the cutoff points were used for futher analysis.

Figure S6

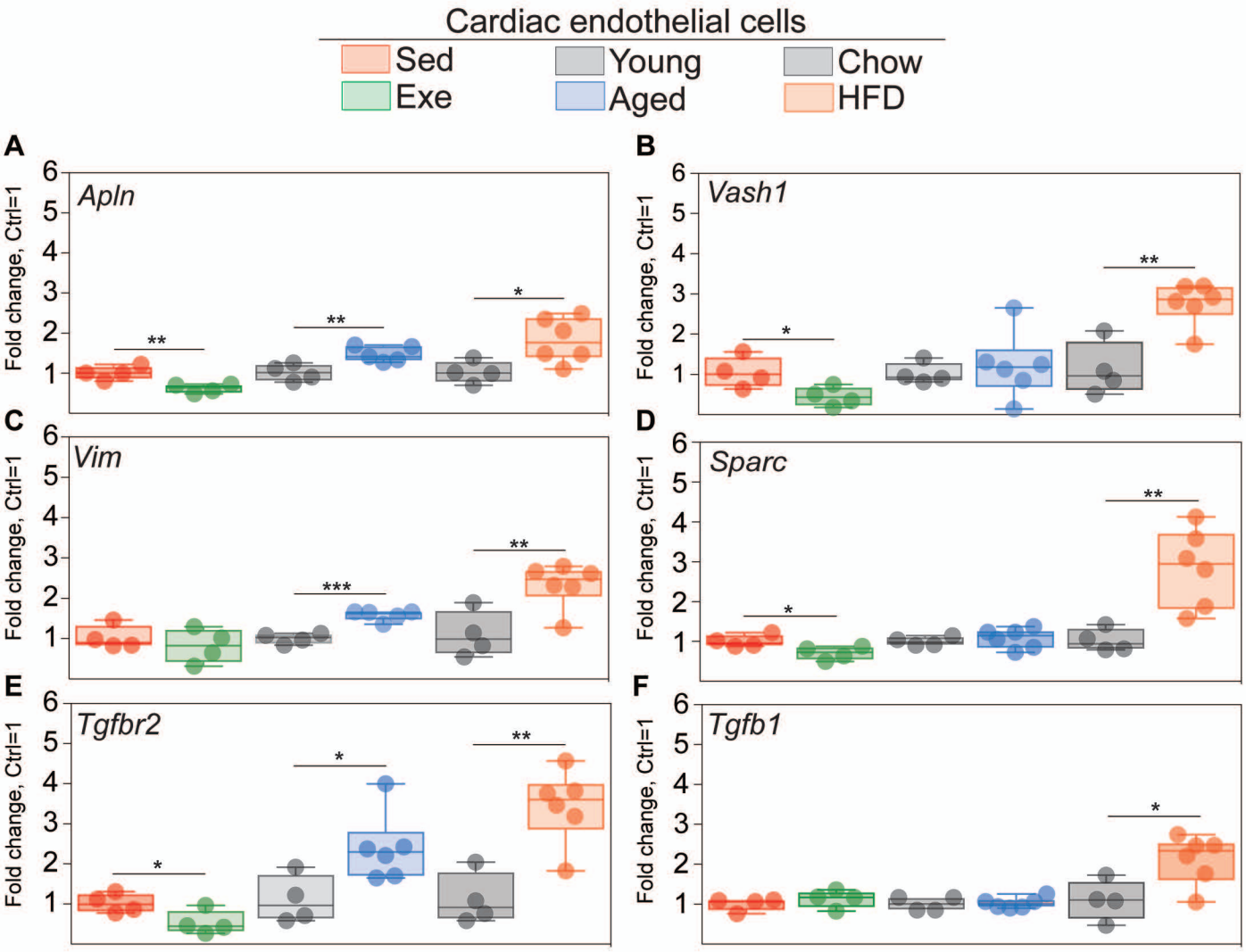

Figure S6. QPCR validation of the indicated genes in the cardiac EC during aging, obesity, exercise training in young and aged mice. **A-F.** mRNA expression of Apln, Vim, Tgfbr2, Vash1, Sparc and Tgfb1 in the cardiac EC of indicated experimental groups (N=4-6/group). Gene expression is normalised to HPRT1 expression. Data is presented as mean ± SEM. Student's t test was used, *p<0.05, **p<0.01, ***p<0.001.

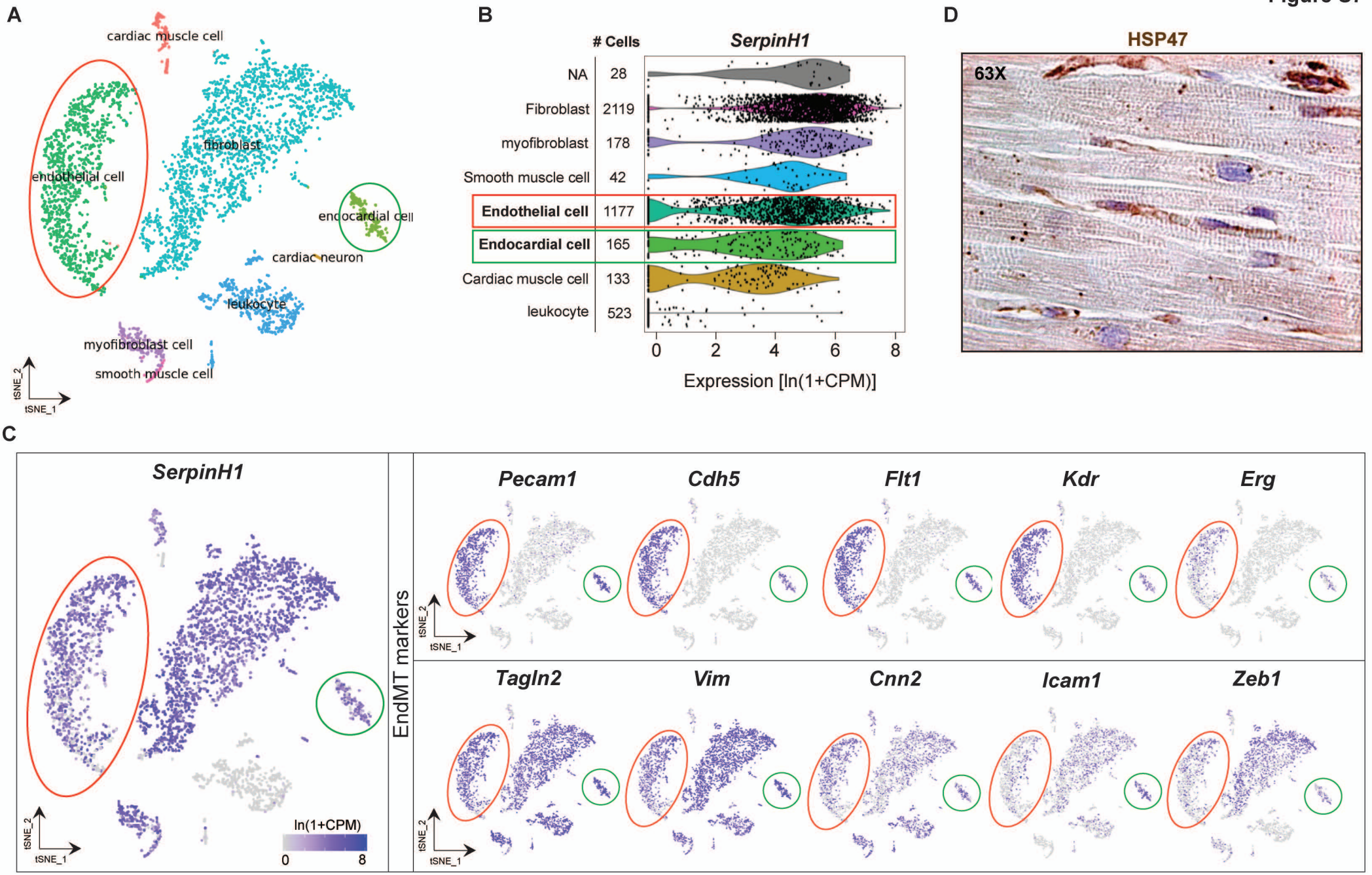

Figure S7. Expression of SerpinH1/HSP47 in different cardiac cell types and in the human heart. A tSNE plot showing **A.** cardiac cell types in the adult mouse heart. **B.** Violin plots showing the levels of SerpinH1 transcripts in fibroblasts, myofibroblasts, smooth muscle cells, endothelial cells, endocardial cells, cardiac muscle cells and leucocytes (each black dot denotes a single cell). **C**. tSNE plot showing the expression of SerpinH1 and EndMT genes in the endothelial cell cluster (cells within red circle) and endocardial cluster (cells within green clusters) Illustrations in the panels A-E were analyzed and acquired from publicly available single cell database Tabula muris: https://tabula-muris.ds.czbiohub.org/. **D.** Representative longitudinal IHC image of human heart demonstrating strong SERPINH1/HSP47 expression in interstitial cells (fibroblasts, endothelial cells) and weak staining within cardiomyocytes. Scale bar 100 µm.

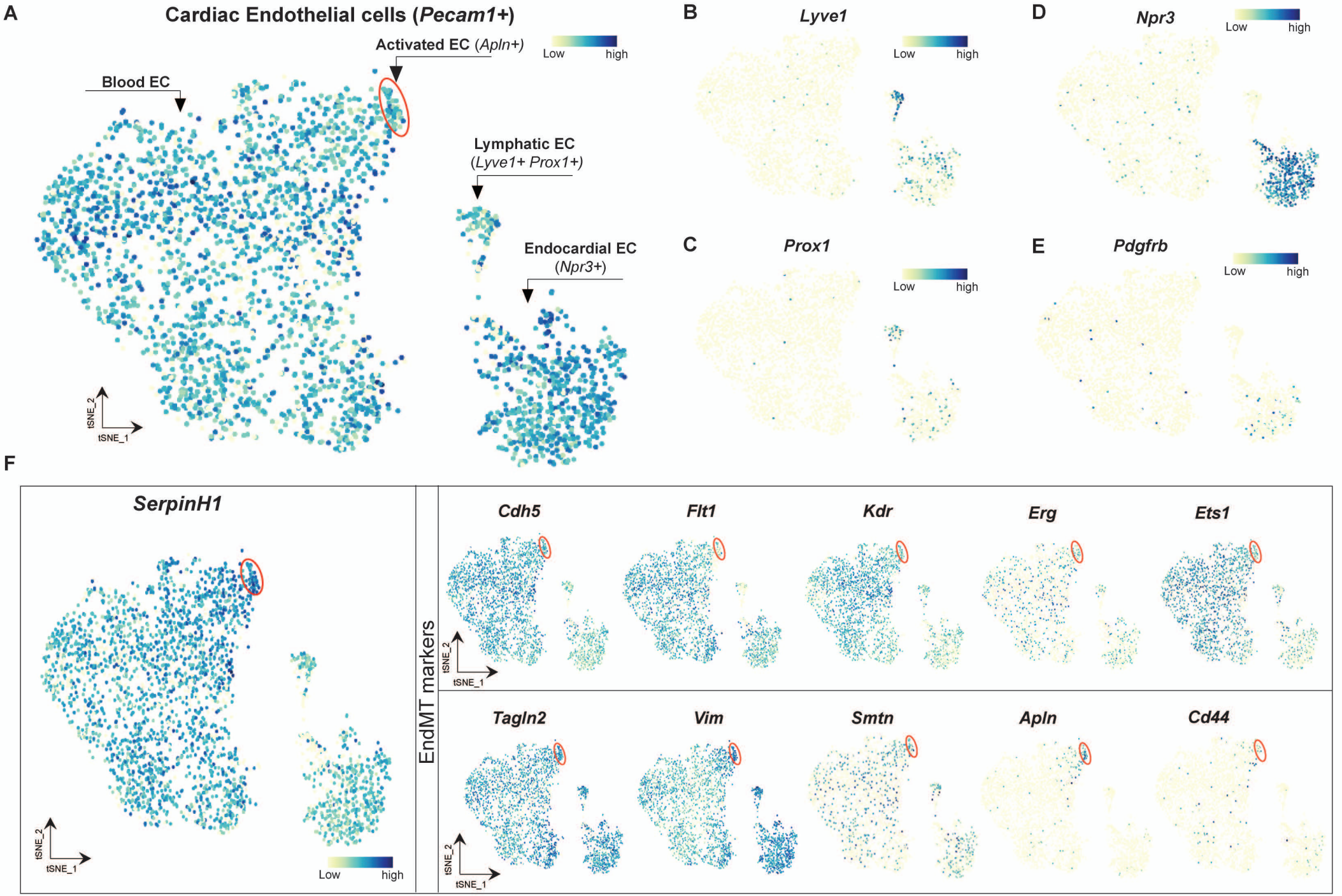

Figure S8. SERPINH1 expression in different subset of cardiac EC. A-D. t-SNE plot showing the Blood EC, Activated EC (Apln+) highlighted within red circle, lymphatic EC (lyve1+ Prox1+) and endocardial EC (Npr3+), **E.** Pdgfrb expression in cardiac EC population, **F.** SerpinH1 is expressed in all endothial cell population, highly expressed in Apln+ activated EC (cell cluster within red circle) which shows decreased expression of EC genes (Cdh5, Flt1, Kdr, Erg and Ets1) and increased expression of Mesenchymal genes (Tagln2, Vim, Smtn, Cd44). Illustration in the panel A-F were analysed from publicly available heart EC atlas from peter carmeliet lab (https://endotheliomics.shinyapps.io/ec_atlas/).

Figure S9

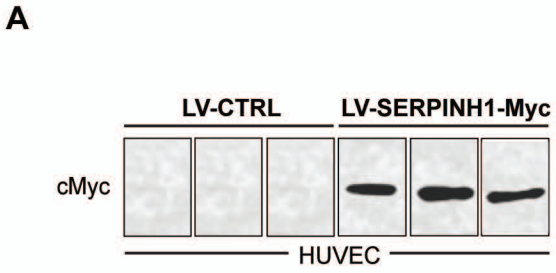

Figure S9. SERPINH1 overexpression in endothelial cells. A. Western blot analysis of cMyc expression in LV-SERPINH1-Myc treated HUVEC (N=3 biological replicates/group).

Supplementary Table 1. Echocardiography measurements of cardiac function and ventricular dimensions.

Experiment groups	IVS,d (mm)	IVS,s (mm)	LVID,d (mm)	LVID,s (mm)	LVPW,d (mm)	LVPW,s (mm)	LV Vol,d (μl)	LV Vol,s (μl)	LV mass (mg)	FS (%)
6 weeks of treadmill running										
EXE (n=5); 3 mo old	1.02±0.14	1.33±0.13	3.84±0.10	2.56±0.12†	0.74±0.05	1.25±0.05	63.8±4.01	23.9±2.73†	103.6±19.1	33.5±2.3
SED (n=5); 3 mo old	0.89±0.07	1.13±0.11	3.93±0.05	2.94±0.10	0.89±0.09	1.22±0.13	67.2±1.85	33.5±2.83	106.9±4.4	25.3±1.9
14 weeks of high fat diet feeding										
HFD (n=5); 3 mo old	1.11±0.04†	1.39±0.06	3.92±0.13	3.10±0.21	0.86±0.03†	1.09±0.08	67.2±5.32	39.3±6.5	121.7±5.2	21.1±3.3†
CHOW (n=5); 3 mo old	0.93±0.05	1.41±0.03	4.19±0.08	2.96±0.08	0.75±0.04	1.05±0.15	78.5±3.54	34.2±2.4	107.9±3.8	29.4±1.6
18 months of aging										
AGED (n=6); 18 mo old	1.05±0.03†	1.39±0.06†	4.16±0.11	3.31±0.13†	1.09±0.06†	1.34±0.06†	77.2±4.4	44.9±4.1†	150.1±9.1†	20.7±1.6†
YOUNG (n=6); 2 mo old	0.85±0.04	1.19±0.06	3.94±0.10	2.84±0.13	0.77±0.06	1.13±0.03	68.1±4.4	31.0±3.3	93.8±3.9	27.9±1.7
Trans-aortic constriction: Week 0-6										
Sham(n=5);Week 0	0.78±0.03	1.12±0.03	3.50±0.06	2.31±0.05	0.79±0.01	1.19±0.03	51.0±2.0	18.2±1.2	73.5±1.6	34.1±0.8
TAC (n=10);Week 0	0.77±0.03	1.10±0.04	3.67±0.12	2.57±0.13	0.81±0.02	1.20±0.03	58.1±5.0	24.8±3.6	80.1±3.1	30.4±1.3
Sham(n=5);Week 1	0.73±0.03	1.07±0.06	3.88±0.09	2.74±0.12	0.75±0.03	1.09±0.05	65.4±3.7	28.4±3.1	80.1±2.2	29.4±1.9
TAC (n=10);Week 1	0.87±0.04†	1.18±0.06	3.92±0.12	3.03±0.18	0.98±0.06†	1.25±0.07	67.6±5.1	37.8±5.0	111.6±7.1†	23.2±2.3
Sham(n=5);Week 2	0.70±0.04	1.07±0.05	3.89±0.06	2.63±0.07	0.76±0.02	1.11±0.04	65.6±2.8	25.6±1.8	79.3±3.2	32.4±1.4
TAC (n=10);Week 2	0.87±0.04†	1.14±0.05	4.12±0.15	3.34±0.21†	1.02±0.03†	1.27±0.04†	76.9±7.3	48.0±7.4†	124.4±6.2†	19.5±2.6†
TAC (n=5); Week 3	0.97±0.04†	1.17±0.04	4.38±0.19†	3.77±0.16	1.08±0.06†	1.29±0.07	87.8±9.8	61.4±6.6†	153.6±12.2†	13.8±0.9†
TAC (n=5); Week 4	0.92±0.05†	1.20±0.06	4.60±0.23†	4.04±0.24	1.25±0.10†	1.37±0.09	99.0±13†	72.8±11†	178.3±9.9	12.4±0.8†
TAC (n=5); Week 5	0.89±0.10†	1.15±0.11	4.92±0.07†	4.40±0.09	1.00±0.05†	1.12±0.03†	114.0±4†	87.8±4.3†	165.6±10	10.6±1.4†
TAC (n=5); Week 6	0.81±0.06	0.96±0.08	5.15±0.22†	4.82±0.24	0.98±0.09†	1.01±0.09	127.8±13†	110.2±13†	164.9±7.9	6.4±0.8†

mo: Months; **IVS,d:** Interventricular septum thickness at end-diastole; **IVS,s:** Interventricular septum thickness at end-systole; **LVID,d:** Left ventricular internal dimension at end-diastole; **LVID,s:** Left ventricular internal dimension at end-systole; **LVPW,d:** Left ventricular posterior wall thickness at end-diastole; **LVPW,s:** Left ventricular posterior wall thickness at end-systole; **LV Vol, d:** Left ventricular volume at end-diastole; **LV Vol,s:** Left ventricular volume at end-systole; **LV mass:** Left ventricular mass; **FS:** Fractional shortening.

Data are mean±SEM. Student *t* test was used, † $p<0.05$.

Supplementary Table 2: List of antibodies used for fluorescence-activated cell sorting (FACS), immunofluorescent staining (IF) and Western blotting (WB).

Antibody	Host	Application	Company/Catalog number
FITC-CD31	Mouse	FACS	Invitrogen/RM5201
Pacificblue-CD45	Mouse	FACS	Biolegend/103125
Pacificblue-Ter119	Mouse	FACS	Biolegend/116231
PE-Cyanine7-CD140a	Mouse	FACS	eBioscience/25-1401
CD16/CD32 (Fc blocker)	Mouse	FACS	BD Biosciences/553142
Mouse CD31	Rat	IF	BD Pharmingen/553370
Human VEcadherin	Rabbit	IF	Cell Signaling/#2500S
Tagln	Sheep	WB/IF	R&D Biosystems/AF7886
c-MYC	Mouse	WB/IF	Thermo Fisher/13-2500
HSP47	Mouse	WB/IHC/IF	Enzo Life Sciences/ADI-SPA-470-D
Collagen 1	Rabbit	IF	Abcam/ab34710
aSMA	Mouse	IF	Sigma-Aldrich/A5228
GAPDH	Mouse	WB	Sigma-Aldrich/CB1001

Supplementary Table 3: List of human shRNA constructs used in the gene silencing studies.

Construct name	Clone ID	Match regions	Target sequence
shSERPINH1(#1)	TRCN0000003590	CDS	CCTCTACAACTACTACGACGA
shSERPINH1(#2)	TRCN0000003594	CDS	GCCTTTGAGTTGGACACAGAT
shSERPINH1(#3)	TRCN0000003593	CDS	CAACTACTACGACGACGAGAA
shSERPINH1(#4)	TRCN0000003591	3'UTR	TCCCAACCTCTCCCAACTATA

Supplementary Table 4: Primer pair sequences for SYBR green and TaqMan real-time qPCR assays.

Gene	Forward primer (5’-3’)	Reverse primer (5’-3’)
hSERPINH1	ATGAGAAATTCCACCACAAGATG	GATCTTCAGCTGCTCTTTGGTTA
hCD31	CTGCTGACCCTTCTGCTCTGTTC	GGCAGGCTCTTCATGTCAACACT
hCDH5	CGTGAGCATCCAGGCAGTGGTAGC	GAGCCGCCGCCGCAGGAAG
hTIE1	ACCCGCTGTGAACAGGCCTGCAGAGA	CTTGGCACTGGCTTCCTCT
hID1	CTGCTCTACGACATGAACGG	GAAGGTCCCTGATGTAGTCGAT
hCYCLIND1	GCGGAGGAGAACAAACAGAT	TGAGGCGGTAGTAGGACAGG
hTAGLN	CGGTTAGGCCAAGGCTCTAC	CCAGCTCCTCGTCATACTTC
hαSMA	AAGCACAGAGCAAAAGAGGAAT	ATGTCGTCCCAGTTGGTGAT
hCD44	TGGCACCCGCTATGTCGAG	GTAGCAGGGATTCTGTCTG
hVIM	CGAGGAGAGCAGGATTTCTC	GGTATCAACCAGAGGGAGTGA
hNOTCH3	ACCGATGTCAACGAGTGTCT	GTTGACACAGGGGCTACTCT
hZEB2	GAGGCGCAAACAAGCCAATC	TCAGAACCTGTGTCCACTAC
hSLUG	ACTCCGAAGCCAAATGACAA	CTCTCTCTGTGGGTGTGTGT
hFN1	CCATAGCTGAGAAGTGTTTTG	CAAGTACAATCTACCATCATCC
hVCAM1	CGCAAACACTTTATGTCAATGTTG	GATTTTCGGAGCAGGAAAGC
hICAM1	TGCCCTGATGGGCAGTCAAC	CCCGTTTCAGCTCCTTCTCC
hHPRT1	TGAGGATTTGGAAAGGGTGT	TCCCCTGTTGACTGGTCATT
hNRARP	Hs01104102_S1	
mCdh5	Mm00486938_m1	
mTie1	Mm00441786_m1	
mSerpinH1	ATGTTCTTTAAGCCACACTG	TCGTCATAGTAGTTGTACAGG
mVwa1	GATGATCTTCCTATCATTGCC	CAATTCCAGCACGTAGTAAC
mVim	CTTGAACGGAAAGTGGAATCCT	GTCAGGCTTGGAAACGTCC

mTgfbr2	TCTTTTCGGAAGAATACZCC	GTAGCAGTAGAAGATGATGATG
mVash1	CAAGGAAATGACCAAAGAGG	ACTGTTGGTGAGGTAAATTC
mSparc	GAACCCACATGGCAAGTCTTA	AAAGCCCAATTGCAGTTGAGT
mTgfb1	CTCCCGTGGCTTCTAGTGC	GCCTTAGTTTGGACAGGATCTG
mApln	CAGGCCTATTCCCAGGCTCA	CAAGATCAAGGGCGCAGTCA

Supplementary Table 5A: Reference list for endothelial and mesenchymal genes indicated in the Figure 4B (EXE vs. SED) heat map.

Gene	Description	Reference #
Malat1	Metastasis Associated Lung Adenocarcinoma Transcript 1	14
Mgp	Matrix Gla Protein	15
Ankrd11	Ankyrin Repeat Domain 11	16
Plcb4	Phospholipase C Beta 4	17
Rock1	Rho Associated Coiled-Coil Containing Protein Kinase 1	18
Adgrg6	Adhesion G Protein-Coupled Receptor G6	19
Ppp4r3a	Protein Phosphatase 4 Regulatory Subunit 3A	20
Phip	Pleckstrin Homology Domain Interacting Protein	21
Clk1	CDC Like Kinase 1	22
Ankrd12	Ankyrin Repeat Domain 12	23
Ppl	Periplakin	24
Krit1	KRIT1 Ankyrin Repeat Containing	25, 26
Calcrl	Calcitonin Receptor Like Receptor	27
Apln	Apelin	28
Aplnr	Apelin Receptor	29
Vash1	Vasohibin 1	30, 31
Fscn1	Fascin Actin-Bundling Protein 1	32
Cd93	CD93 Molecule	33, 34
Vwa1	Von Willebrand Factor A Domain Containing 1	35, 36

Adamts4	ADAM Metallopeptidase With Thrombospondin Type 1 Motif 4	37
Sparc	Secreted Protein Acidic And Cysteine Rich	38
Col4a2	Collagen Type IV Alpha 2 Chain	39, 40
Cd34	CD34 Molecule	41, 42
Tuba1a	Tubulin Alpha 1a	43
Cx3cl1	C-X3-C Motif Chemokine Ligand 1	44
Mest	Mesoderm Specific Transcript	45
Cnn2	Calponin 2	46
Cd44	CD44 Molecule (Indian Blood Group)	47
Trp53	Tumor Protein P53	48
Prex1	Phosphatidylinositol-3,4,5-Trisphosphate Dependent Rac Exchange Factor 1	49
Hspg2	Heparan Sulfate Proteoglycan 2	29
Tnfaip1	TNF Alpha Induced Protein 1	50
Lamb1	Laminin Subunit Beta 1	51
Ltbp4	Latent Transforming Growth Factor Beta Binding Protein 4	52
Sept4	Septin 4	53
Unc5b	Unc-5 Netrin Receptor B	54

Supplementary Table 5B: Reference list for endothelial and mesenchymal genes indicated in the Figure 4C (Aged vs. Young) heat map.

Gene	Description	Reference #
Npr3	Natriuretic Peptide Receptor 3	55, 56
Tagln2	Transgelin 2	57
Vim	Vimentin	58
Msn	Moesin	59-61
Socs5	Suppressor Of Cytokine Signaling 5	62
Vcam1	Vascular adhesion molecule 1	63
Notch4	Notch Receptor 4	41, 64
Stat6	Signal Transducer And Activator Of Transcription 6	65
Adamtsl4	ADAMTS Like 4	66
Jag2	Jagged Canonical Notch Ligand 2	41
Cdh13	Cadherin 13	67, 68
Hif1a	Hypoxia Inducible Factor 1 Subunit Alpha	41
Ism1	Isthmin 1	69, 70
Tbx3	T-Box Transcription Factor 3	71
Tgfa	Transforming Growth Factor Alpha	72
Furin	Furin, Paired Basic Amino Acid Cleaving Enzyme	73
Eng	Endoglin	74, 75
Smad6	SMAD Family Member 6	76, 77
Smad7	SMAD Family Member 7	76, 77
Sox17	SRY-Box Transcription Factor 17	78

Tead1	TEA Domain Transcription Factor 1	41, 79
Tead2	TEA Domain Transcription Factor 2	41, 79
Klf3	Kruppel Like Factor 3	80, 81
Klf4	Kruppel Like Factor 4	82
Sulf1	Sulfatase 1	83
Wt1	WT1 Transcription Factor	84, 85
Ankrd1	Ankyrin Repeat Domain 1	86, 87
Cd247	CD247 Molecule	88
Hbegf	Heparin Binding EGF Like Growth Factor	89
Vegfc	Vascular Endothelial Growth Factor C	82, 90
Nos2	Nitric Oxide Synthase 2	91
Nrarp	NOTCH Regulated Ankyrin Repeat Protein	92
Rgs2	Regulator of G Protein Signaling 2	93
Cldn5	Claudin 5	94
Kit	KIT Proto-Oncogene, Receptor Tyrosine Kinase	95
Cd200	CD200 Molecule	96
Gja4	Gap Junction Protein Alpha 4	97, 98
Nog	Noggin	99, 100
Ets1	Ets Proto-Oncogene 1, Transcription factor	101, 102
Hes1	Hes Family BHLH Transcription Factor 1	103

Supplementary Table 5C: Reference list for endothelial and mesenchymal genes indicated in the Figure 4D (HFD vs. Chow) heat map.

Gene	Description	Reference #
Apln	Apelin	28
Vwa1	Von Willebrand Factor A Domain Containing 1	35, 36
Tuba1a	Tubulin Alpha 1a	43
Ezh2	Enhancer Of Zeste 2 Polycomb Repressive Complex 2 Subunit	86
Fsd2	Fibronectin Type III And SPRY Domain Containing 2	104-106
Mest	Mesoderm Specific Transcript	45
Angptl4	Angiopoietin Like 4	107
Me1	Malic Enzyme 1	108
Cldn5	Claudin 5	94
Ankrd1	Ankyrin Repeat Domain 1	86, 87
E2f1	E2F Transcription Factor 1	109
Hey1	Hes Related Family BHLH Transcription Factor With YRPW Motif 1	64, 110
Fndc5	Fibronectin Type III Domain Containing 5	111
Dsp	Desmoplakin	112
Trp53inp2	Tumor Protein P53 Inducible Nuclear Protein 2	113
Cd36	CD36 Molecule	114
Hist4h4	Histone H4	86, 110
Xbp1	X-Box Binding Protein 1	115
Inhbb	Inhibin Subunit Beta B	116
Podxl	Podocalyxin Like	117

Egr1	Early Growth Response 1	118
L1cam	L1 Cell Adhesion Molecule	119
Rarg	Retinoic Acid Receptor Gamma	120
Ace	Angiotensin I Converting Enzyme	121
Apoe	Apolipoprotein E	122
Mkl2	Myocardin-like protein 2	123
Tln2	Talin 2	124
Pdgfrb	Platelet Derived Growth Factor Receptor Beta	125
Igfbp3	Insulin Like Growth Factor Binding Protein 3	126

Supplementary Table 5D: Reference list for endothelial and mesenchymal genes indicated in the Figure 4E (TAC (2) vs. Sham) heat map.

Gene	Description	Reference #
Spry4	Sprouty RTK Signalling Antagonists	127
Mmp14	Matrix Metallopeptidase 14	128
Tnc	Tenascin C	129, 130
Fn1	Fibronectin 1	131
Vim	Vimentin	132
Emilin1	Elastin Microfibril Interfacer 1	133, 134
Col4a1	Collagen Type IV Alpha 1 Chain	40
Tgfb1	Transforming Growth Factor Beta 1	135, 136
Tgfbr2	Transforming Growth Factor Beta Receptor 2	135, 136
Ltbp3	Latent Transforming Growth Factor Beta Binding Protein 3	52
Bmp2	Bone Morphogenetic Protein 2	137
Lamb1	Laminin Subunit Beta 1	51
Msn	Moesin	60, 61
Sele	Selectin E	138
Acta1	Alpha-Actin-1	139
Tagln2	Transgelin 2	57
Hif1a	Hypoxia Inducible Factor 1 Subunit Alpha	41
Adamts4	ADAM Metallopeptidase With Thrombospondin Type 1 Motif 4	37
Nrp2	Neuropilin 2	140
Esm1	Endothelial Cell Specific Molecule 1	141-143
Apln	Apelin	28
Cd34	CD34 Molecule	144, 145

Vash1	Vasohibin 1	30, 31
Vwa1	Von Willebrand Factor A Domain Containing 1	35, 36
Epas1	Endothelial PAS Domain Protein 1	146
Apoe	Apolipoprotein E	122
Angpt2	Angiopoietin	147
Id2	Inhibitor of DNA Binding 2	148
Id3	Inhibitor of DNA Binding 3, HLH protein	148
Efnb1	Ephrin B1	149
Igf1r	Insulin Like Growth Factor 1 Receptor	150

Supplementary Table 5E: Reference list for endothelial and mesenchymal genes indicated in the Figure 4F (TAC (7) vs. Sham) heat map.

Gene	Description	Reference #
Spry4	Sprouty RTK Signaling Antagonist 4	127
Esm1	Endothelial Cell Specific Molecule 1	141-143
Epha2	EPH Receptor A2	149
Socs5	Suppressor Of Cytokine Signaling 5	62
Sele	Selectin E	138
Acta1	Alpha-Actin-1	139
Nostrin	Nitric Oxide Synthase Trafficking	151
Esam	Endothelial Cell Adhesion Molecule	152
Cd34	CD34 molecule	144, 145
Tgfb1	Transforming Growth Factor Beta 1	135, 136
Tnfaip2	TNF Alpha Induced Protein 2	153
Ankrd1	Ankyrin Repeat Domain 1	86, 87
Mmp14	Matrix Metallopeptidase 14	128
Vwf	Von Willebrand Factor	154
Col4a1	Collagen Type IV Alpha 1 Chain	39, 40
Tnc	Tenascin C	129, 130
Col4a2	Collagen Type IV Alpha 2 Chain	39, 40
Stat3	Signal Transducer And Activator Of Transcription 3	155
Ecm1	Extracellular Matrix Protein 1	156
Zeb1	Zinc Finger E-Box Binding Homeobox 1	155
Emilin1	Elastin Microfibril Interfacer 1	133, 134
Sparc	Secreted Protein Acidic And Cysteine Rich	38

Dsp	Desmoplakin	112
Notch3	NOTCH Receptor 3	125, 157
Pdgfrb	Platelet Derived Growth Factor Receptor Beta	125
Epha4	EPH Receptor 4	149
Ddr2	Discoidin Domain Receptor Tyrosine Kinase 2	158
Zeb2	Zinc Finger E-Box Binding Homeobox 2	82
Apoe	Apolipoprotein E	122
Sox7	SRY-Box Transcription Factor 7	159
Cxcl9	C-X-C Motif Chemokine Ligand 9	160

References

1.Kivela R, Hemanthakumar KA, Vaparanta K, Robciuc M, Izumiya Y, Kidoya H, Takakura N, Peng X, Sawyer DB, Elenius K, Walsh K and Alitalo K. Endothelial Cells Regulate Physiological Cardiomyocyte Growth via VEGFR2-Mediated Paracrine Signaling. *Circulation*. 2019;139:2570-2584.

2.Kallio MA, Tuimala JT, Hupponen T, Klemela P, Gentile M, Scheinin I, Koski M, Kaki J and Korpelainen EI. Chipster: user-friendly analysis software for microarray and other high-throughput data. *BMC Genomics*. 2011;12:507.

3.Bolger AM, Lohse M and Usadel B. Trimmomatic: a flexible trimmer for Illumina sequence data. *Bioinformatics*. 2014;30:2114-20.

4.Kim D, Langmead B and Salzberg SL. HISAT: a fast spliced aligner with low memory requirements. *Nat Methods*. 2015;12:357-60.

5.Anders S, Pyl PT and Huber W. HTSeq--a Python framework to work with high-throughput sequencing data. *Bioinformatics*. 2015;31:166-9.

6.Love MI, Huber W and Anders S. Moderated estimation of fold change and dispersion for RNA-seq data with DESeq2. *Genome Biol*. 2014;15:550.

7.Mi H, Muruganujan A, Huang X, Ebert D, Mills C, Guo X and Thomas PD. Protocol Update for large-scale genome and gene function analysis with the PANTHER classification system (v.14.0). *Nat Protoc*. 2019;14:703-721.

8.Meinken J, Walker G, Cooper CR and Min XJ. MetazSecKB: the human and animal secretome and subcellular proteome knowledgebase. *Database (Oxford)*. 2015;2015.

9.Almagro Armenteros JJ, Salvatore M, Emanuelsson O, Winther O, von Heijne G, Elofsson A and Nielsen H. Detecting sequence signals in targeting peptides using deep learning. *Life Sci Alliance*. 2019;2.

10.Bendtsen JD, Jensen LJ, Blom N, Von Heijne G and Brunak S. Feature-based prediction of non-classical and leaderless protein secretion. *Protein Eng Des Sel*. 2004;17:349-56.

11.Lois C, Hong EJ, Pease S, Brown EJ and Baltimore D. Germline transmission and tissue-specific expression of transgenes delivered by lentiviral vectors. *Science*. 2002;295:868-72.

12.Evrard SM, Lecce L, Michelis KC, Nomura-Kitabayashi A, Pandey G, Purushothaman KR, d'Escamard V, Li JR, Hadri L, Fujitani K, Moreno PR, Benard L, Rimmele P, Cohain A, Mecham B, Randolph GJ, Nabel EG, Hajjar R, Fuster V, Boehm M and Kovacic JC. Endothelial to mesenchymal transition is common in atherosclerotic lesions and is associated with plaque instability. *Nat Commun*. 2016;7:11853.

13.Magenta A, Cencioni C, Fasanaro P, Zaccagnini G, Greco S, Sarra-Ferraris G, Antonini A, Martelli F and Capogrossi MC. miR-200c is upregulated by oxidative stress and induces endothelial cell apoptosis and senescence via ZEB1 inhibition. *Cell Death Differ*. 2011;18:1628-39.

14.Michalik KM, You X, Manavski Y, Doddaballapur A, Zornig M, Braun T, John D, Ponomareva Y, Chen W, Uchida S, Boon RA and Dimmeler S. Long noncoding RNA MALAT1 regulates endothelial cell function and vessel growth. *Circ Res*. 2014;114:1389-97.

15.Bostrom K, Zebboudj AF, Yao Y, Lin TS and Torres A. Matrix GLA protein stimulates VEGF expression through increased transforming growth factor-beta1 activity in endothelial cells. *J Biol Chem*. 2004;279:52904-13.

16.Neilsen PM, Cheney KM, Li CW, Chen JD, Cawrse JE, Schulz RB, Powell JA, Kumar R and Callen DF. Identification of ANKRD11 as a p53 coactivator. *J Cell Sci*. 2008;121:3541-52.

17.Rhee SG and Bae YS. Regulation of phosphoinositide-specific phospholipase C isozymes. *J Biol Chem*. 1997;272:15045-8.

18.Lisowska J, Rodel CJ, Manet S, Miroshnikova YA, Boyault C, Planus E, De Mets R, Lee HH, Destaing O, Mertani H, Boulday G, Tournier-Lasserve E, Balland M, Abdelilah-Seyfried S, Albiges-Rizo C and Faurobert E. The CCM1-CCM2 complex controls complementary functions of ROCK1 and ROCK2 that are required for endothelial integrity. *J Cell Sci*. 2018;131.

19.Wu S, Ou T, Xing N, Lu J, Wan S, Wang C, Zhang X, Yang F, Huang Y and Cai Z. Whole-genome sequencing identifies ADGRG6 enhancer mutations and FRS2 duplications as angiogenesis-related drivers in bladder cancer. *Nat Commun*. 2019;10:720.

20.Kim BR, Seo SH, Park MS, Lee SH, Kwon Y and Rho SB. sMEK1 inhibits endothelial cell proliferation by attenuating VEGFR-2-dependent-Akt/eNOS/HIF-1alpha signaling pathways. *Oncotarget*. 2015;6:31830-43.

21.Farhang-Fallah J, Yin X, Trentin G, Cheng AM and Rozakis-Adcock M. Cloning and characterization of PHIP, a novel insulin receptor substrate-1 pleckstrin homology domain interacting protein. *J Biol Chem*. 2000;275:40492-7.

22.Bowler E, Porazinski S, Uzor S, Thibault P, Durand M, Lapointe E, Rouschop KMA, Hancock J, Wilson I and Ladomery M. Hypoxia leads to significant changes in alternative splicing and elevated expression of CLK splice factor kinases in PC3 prostate cancer cells. *BMC Cancer*. 2018;18:355.

23.Bai R, Li D, Shi Z, Fang X, Ge W and Zheng S. Clinical significance of Ankyrin repeat domain 12 expression in colorectal cancer. *J Exp Clin Cancer Res*. 2013;32:35.

24.Besnard V, Dagher R, Madjer T, Joannes A, Jaillet M, Kolb M, Bonniaud P, Murray LA, Sleeman MA and Crestani B. Identification of periplakin as a major regulator of lung injury and repair in mice. *JCI Insight*. 2018;3.

25.Zhou Z, Tang AT, Wong WY, Bamezai S, Goddard LM, Shenkar R, Zhou S, Yang J, Wright AC, Foley M, Arthur JS, Whitehead KJ, Awad IA, Li DY, Zheng X and Kahn ML.

Cerebral cavernous malformations arise from endothelial gain of MEKK3-KLF2/4 signalling. *Nature*. 2016;532:122-6.

26.Bravi L, Malinverno M, Pisati F, Rudini N, Cuttano R, Pallini R, Martini M, Larocca LM, Locatelli M, Levi V, Bertani GA, Dejana E and Lampugnani MG. Endothelial Cells Lining Sporadic Cerebral Cavernous Malformation Cavernomas Undergo Endothelial-to-Mesenchymal Transition. *Stroke*. 2016;47:886-90.

27.Dackor RT, Fritz-Six K, Dunworth WP, Gibbons CL, Smithies O and Caron KM. Hydrops fetalis, cardiovascular defects, and embryonic lethality in mice lacking the calcitonin receptor-like receptor gene. *Mol Cell Biol*. 2006;26:2511-8.

28.Wysocka MB, Pietraszek-Gremplewicz K and Nowak D. The Role of Apelin in Cardiovascular Diseases, Obesity and Cancer. *Front Physiol*. 2018;9:557.

29.Apostolidis SA, Stifano G, Tabib T, Rice LM, Morse CM, Kahaleh B and Lafyatis R. Single Cell RNA Sequencing Identifies HSPG2 and APLNR as Markers of Endothelial Cell Injury in Systemic Sclerosis Skin. *Front Immunol*. 2018;9:2191.

30.Watanabe K, Hasegawa Y, Yamashita H, Shimizu K, Ding Y, Abe M, Ohta H, Imagawa K, Hojo K, Maki H, Sonoda H and Sato Y. Vasohibin as an endothelium-derived negative feedback regulator of angiogenesis. *J Clin Invest*. 2004;114:898-907.

31.Sato Y. The vasohibin family: a novel family for angiogenesis regulation. *J Biochem*. 2013;153:5-11.

32.Wang CQ, Tang CH, Wang Y, Jin L, Wang Q, Li X, Hu GN, Huang BF, Zhao YM and Su CM. FSCN1 gene polymorphisms: biomarkers for the development and progression of breast cancer. *Sci Rep*. 2017;7:15887.

33.Galvagni F, Nardi F, Maida M, Bernardini G, Vannuccini S, Petraglia F, Santucci A and Orlandini M. CD93 and dystroglycan cooperation in human endothelial cell adhesion and migration adhesion and migration. *Oncotarget*. 2016;7:10090-103.

34.Lugano R, Vemuri K, Yu D, Bergqvist M, Smits A, Essand M, Johansson S, Dejana E and Dimberg A. CD93 promotes beta1 integrin activation and fibronectin fibrillogenesis during tumor angiogenesis. *J Clin Invest*. 2018;128:3280-3297.

35.Fitzgerald J. WARP: A Unique Extracellular Matrix Component of Cartilage, Muscle, and Endothelial Cell Basement Membranes. *Anat Rec (Hoboken)*. 2019.

36.Deckx S, Carai P, Bateman J, Heymans S and Papageorgiou AP. Breeding Strategy Determines Rupture Incidence in Post-Infarct Healing WARPing Cardiovascular Research. *PLoS One*. 2015;10:e0139199.

37.Hsu YP, Staton CA, Cross N and Buttle DJ. Anti-angiogenic properties of ADAMTS-4 in vitro. *Int J Exp Pathol*. 2012;93:70-7.

38.Fenouille N, Tichet M, Dufies M, Pottier A, Mogha A, Soo JK, Rocchi S, Mallavialle A, Galibert MD, Khammari A, Lacour JP, Ballotti R, Deckert M and Tartare-Deckert S. The epithelial-mesenchymal transition (EMT) regulatory factor SLUG (SNAI2) is a downstream target of SPARC and AKT in promoting melanoma cell invasion. *PLoS One*. 2012;7:e40378.

39.Katsuda S, Okada Y, Minamoto T, Oda Y, Matsui Y and Nakanishi I. Collagens in human atherosclerosis. Immunohistochemical analysis using collagen type-specific antibodies. *Arterioscler Thromb*. 1992;12:494-502.

40.Yang W, Ng FL, Chan K, Pu X, Poston RN, Ren M, An W, Zhang R, Wu J, Yan S, Situ H, He X, Chen Y, Tan X, Xiao Q, Tucker AT, Caulfield MJ and Ye S. Coronary-Heart-Disease-Associated Genetic Variant at the COL4A1/COL4A2 Locus Affects COL4A1/COL4A2 Expression, Vascular Cell Survival, Atherosclerotic Plaque Stability and Risk of Myocardial Infarction. *PLoS Genet*. 2016;12:e1006127.

41.Sanchez-Duffhues G, Garcia de Vinuesa A and Ten Dijke P. Endothelial-to-mesenchymal transition in cardiovascular diseases: Developmental signaling pathways gone awry. *Dev Dyn*. 2018;247:492-508.

42.Kitao A, Sato Y, Sawada-Kitamura S, Harada K, Sasaki M, Morikawa H, Shiomi S, Honda M, Matsui O and Nakanuma Y. Endothelial to mesenchymal transition via transforming growth factor-beta1/Smad activation is associated with portal venous stenosis in idiopathic portal hypertension. *Am J Pathol*. 2009;175:616-26.

43.Groger CJ, Grubinger M, Waldhor T, Vierlinger K and Mikulits W. Meta-analysis of gene expression signatures defining the epithelial to mesenchymal transition during cancer progression. *PLoS One*. 2012;7:e51136.

44.Imaizumi T, Yoshida H and Satoh K. Regulation of CX3CL1/fractalkine expression in endothelial cells. *J Atheroscler Thromb*. 2004;11:15-21.

45.Mayer W, Hemberger M, Frank HG, Grummer R, Winterhager E, Kaufmann P and Fundele R. Expression of the imprinted genes MEST/Mest in human and murine placenta suggests a role in angiogenesis. *Dev Dyn*. 2000;217:1-10.

46.Liu R and Jin JP. Calponin isoforms CNN1, CNN2 and CNN3: Regulators for actin cytoskeleton functions in smooth muscle and non-muscle cells. *Gene*. 2016;585:143-153.

47.Cho SH, Park YS, Kim HJ, Kim CH, Lim SW, Huh JW, Lee JH and Kim HR. CD44 enhances the epithelial-mesenchymal transition in association with colon cancer invasion. *Int J Oncol*. 2012;41:211-8.

48.Choi SH, Kim AR, Nam JK, Kim JM, Kim JY, Seo HR, Lee HJ, Cho J and Lee YJ. Tumour-vasculature development via endothelial-to-mesenchymal transition after radiotherapy controls CD44v6(+) cancer cell and macrophage polarization. *Nat Commun*. 2018;9:5108.

49.Naikawadi RP, Cheng N, Vogel SM, Qian F, Wu D, Malik AB and Ye RD. A critical role for phosphatidylinositol (3,4,5)-trisphosphate-dependent Rac exchanger 1 in endothelial junction disruption and vascular hyperpermeability. *Circ Res*. 2012;111:1517-27.

50.Wolf FW, Marks RM, Sarma V, Byers MG, Katz RW, Shows TB and Dixit VM. Characterization of a novel tumor necrosis factor-alpha-induced endothelial primary response gene. *J Biol Chem*. 1992;267:1317-26.

51.Wagner JUG, Chavakis E, Rogg EM, Muhly-Reinholz M, Glaser SF, Gunther S, John D, Bonini F, Zeiher AM, Schaefer L, Hannocks MJ, Boon RA and Dimmeler S. Switch in Laminin beta2 to Laminin beta1 Isoforms During Aging Controls Endothelial Cell Functions-Brief Report. *Arterioscler Thromb Vasc Biol*. 2018;38:1170-1177.

52.Goumans MJ and Ten Dijke P. TGF-beta Signaling in Control of Cardiovascular Function. *Cold Spring Harb Perspect Biol*. 2018;10.

53.Neubauer K, Neubauer B, Seidl M and Zieger B. Characterization of septin expression in normal and fibrotic kidneys. *Cytoskeleton (Hoboken)*. 2019;76:143-153.

54.Lu X, Le Noble F, Yuan L, Jiang Q, De Lafarge B, Sugiyama D, Breant C, Claes F, De Smet F, Thomas JL, Autiero M, Carmeliet P, Tessier-Lavigne M and Eichmann A. The netrin receptor UNC5B mediates guidance events controlling morphogenesis of the vascular system. *Nature*. 2004;432:179-86.

55.Tang J, Zhang H, He L, Huang X, Li Y, Pu W, Yu W, Zhang L, Cai D, Lui KO and Zhou B. Genetic Fate Mapping Defines the Vascular Potential of Endocardial Cells in the Adult Heart. *Circ Res*. 2018;122:984-993.

56.Zhang H, Huang X, Liu K, Tang J, He L, Pu W, Liu Q, Li Y, Tian X, Wang Y, Zhang L, Yu Y, Wang H, Hu R, Wang F, Chen T, Wang QD, Qiao Z, Zhang L, Lui KO and Zhou B. Fibroblasts in an endocardial fibroelastosis disease model mainly originate from mesenchymal derivatives of epicardium. *Cell Res*. 2017;27:1157-1177.

57.Xiao Y, Li Y, Han J, Pan Y, Tie L and Li X. Transgelin 2 participates in lovastatin-induced anti-angiogenic effects in endothelial cells through a phosphorylated myosin light chain-related mechanism. *PLoS One*. 2012;7:e46510.

58.Piera-Velazquez S and Jimenez SA. Endothelial to Mesenchymal Transition: Role in Physiology and in the Pathogenesis of Human Diseases. *Physiol Rev*. 2019;99:1281-1324.

59.Adyshev DM, Dudek SM, Moldobaeva N, Kim KM, Ma SF, Kasa A, Garcia JG and Verin AD. Ezrin/radixin/moesin proteins differentially regulate endothelial hyperpermeability after thrombin. *Am J Physiol Lung Cell Mol Physiol*. 2013;305:L240-55.

60.Haynes J, Srivastava J, Madson N, Wittmann T and Barber DL. Dynamic actin remodeling during epithelial-mesenchymal transition depends on increased moesin expression. *Mol Biol Cell*. 2011;22:4750-64.

61.Lamouille S, Xu J and Derynck R. Molecular mechanisms of epithelial-mesenchymal transition. *Nat Rev Mol Cell Biol*. 2014;15:178-96.

62.Linossi EM, Chandrashekaran IR, Kolesnik TB, Murphy JM, Webb AI, Willson TA, Kedzierski L, Bullock AN, Babon JJ, Norton RS, Nicola NA and Nicholson SE. Suppressor of Cytokine Signaling (SOCS) 5 utilises distinct domains for regulation of JAK1 and interaction with the adaptor protein Shc-1. *PLoS One*. 2013;8:e70536.

63.Yousef H, Czupalla CJ, Lee D, Chen MB, Burke AN, Zera KA, Zandstra J, Berber E, Lehallier B, Mathur V, Nair RV, Bonanno LN, Yang AC, Peterson T, Hadeiba H, Merkel T, Korbelin J, Schwaninger M, Buckwalter MS, Quake SR, Butcher EC and Wyss-Coray T. Aged blood impairs hippocampal neural precursor activity and activates microglia via brain endothelial cell VCAM1. *Nat Med*. 2019;25:988-1000.

64.Niessen K, Fu Y, Chang L, Hoodless PA, McFadden D and Karsan A. Slug is a direct Notch target required for initiation of cardiac cushion cellularization. *J Cell Biol*. 2008;182:315-25.

65.Nishimura Y, Nitto T, Inoue T and Node K. STAT6 mediates apoptosis of human coronary arterial endothelial cells by interleukin-13. *Hypertens Res*. 2008;31:535-41.

66.Hubmacher D and Apte SS. ADAMTS proteins as modulators of microfibril formation and function. *Matrix Biol*. 2015;47:34-43.

67.Serbanovic-Canic J, de Luca A, Warboys C, Ferreira PF, Luong LA, Hsiao S, Gauci I, Mahmoud M, Feng S, Souilhol C, Bowden N, Ashton JP, Walczak H, Firmin D, Krams R, Mason JC, Haskard DO, Sherwin S, Ridger V, Chico TJ and Evans PC. Zebrafish Model for Functional Screening of Flow-Responsive Genes. *Arterioscler Thromb Vasc Biol*. 2017;37:130-143.

68.Souilhol C, Serbanovic-Canic J, Fragiadaki M, Chico TJ, Ridger V, Roddie H and Evans PC. Endothelial responses to shear stress in atherosclerosis: a novel role for developmental genes. *Nat Rev Cardiol*. 2020;17:52-63.

69.Xiang W, Ke Z, Zhang Y, Cheng GH, Irwan ID, Sulochana KN, Potturi P, Wang Z, Yang H, Wang J, Zhuo L, Kini RM and Ge R. Isthmin is a novel secreted angiogenesis inhibitor that inhibits tumour growth in mice. *J Cell Mol Med*. 2011;15:359-74.

70.Venugopal S, Chen M, Liao W, Er SY, Wong WS and Ge R. Isthmin is a novel vascular permeability inducer that functions through cell-surface GRP78-mediated Src activation. *Cardiovasc Res*. 2015;107:131-42.

71.Mesbah K, Harrelson Z, Theveniau-Ruissy M, Papaioannou VE and Kelly RG. Tbx3 is required for outflow tract development. *Circ Res*. 2008;103:743-50.

72.Valverius EM, Bates SE, Stampfer MR, Clark R, McCormick F, Salomon DS, Lippman ME and Dickson RB. Transforming growth factor alpha production and epidermal growth factor receptor expression in normal and oncogene transformed human mammary epithelial cells. *Mol Endocrinol*. 1989;3:203-14.

73.Yakala GK, Cabrera-Fuentes HA, Crespo-Avilan GE, Rattanasopa C, Burlacu A, George BL, Anand K, Mayan DC, Corliano M, Hernandez-Resendiz S, Wu Z, Schwerk AMK, Tan ALJ, Trigueros-Motos L, Chevre R, Chua T, Kleemann R, Liehn EA, Hausenloy DJ, Ghosh

S and Singaraja RR. FURIN Inhibition Reduces Vascular Remodeling and Atherosclerotic Lesion Progression in Mice. *Arterioscler Thromb Vasc Biol*. 2019;39:387-401.

74.ten Dijke P, Goumans MJ and Pardali E. Endoglin in angiogenesis and vascular diseases. *Angiogenesis*. 2008;11:79-89.

75.van Meeteren LA and ten Dijke P. Regulation of endothelial cell plasticity by TGF-beta. *Cell Tissue Res*. 2012;347:177-86.

76.Topper JN, Cai J, Qiu Y, Anderson KR, Xu YY, Deeds JD, Feeley R, Gimeno CJ, Woolf EA, Tayber O, Mays GG, Sampson BA, Schoen FJ, Gimbrone MA, Jr. and Falb D. Vascular MADs: two novel MAD-related genes selectively inducible by flow in human vascular endothelium. *Proc Natl Acad Sci U S A*. 1997;94:9314-9.

77.Lebrin F, Deckers M, Bertolino P and Ten Dijke P. TGF-beta receptor function in the endothelium. *Cardiovasc Res*. 2005;65:599-608.

78.Goveia J, Zecchin A, Rodriguez FM, Moens S, Stapor P and Carmeliet P. Endothelial cell differentiation by SOX17: promoting the tip cell or stalking its neighbor instead? *Circ Res*. 2014;115:205-7.

79.Zhang H, Liu CY, Zha ZY, Zhao B, Yao J, Zhao S, Xiong Y, Lei QY and Guan KL. TEAD transcription factors mediate the function of TAZ in cell growth and epithelial-mesenchymal transition. *J Biol Chem*. 2009;284:13355-62.

80.Dunn J, Qiu H, Kim S, Jjingo D, Hoffman R, Kim CW, Jang I, Son DJ, Kim D, Pan C, Fan Y, Jordan IK and Jo H. Flow-dependent epigenetic DNA methylation regulates endothelial gene expression and atherosclerosis. *J Clin Invest*. 2014;124:3187-99.

81.Sweet DR, Fan L, Hsieh PN and Jain MK. Kruppel-Like Factors in Vascular Inflammation: Mechanistic Insights and Therapeutic Potential. *Front Cardiovasc Med*. 2018;5:6.

82.Kovacic JC, Dimmeler S, Harvey RP, Finkel T, Aikawa E, Krenning G and Baker AH. Endothelial to Mesenchymal Transition in Cardiovascular Disease: JACC State-of-the-Art Review. *J Am Coll Cardiol*. 2019;73:190-209.

83.Glaser SF, Heumuller AW, Tombor L, Hofmann P, Muhly-Reinholz M, Fischer A, Gunther S, Kokot KE, Hassel D, Kumar S, Jo H, Boon RA, Abplanalp W, John D, Boeckel JN and Dimmeler S. The histone demethylase JMJD2B regulates endothelial-to-mesenchymal transition. *Proc Natl Acad Sci U S A*. 2020;117:4180-4187.

84.von Gise A, Zhou B, Honor LB, Ma Q, Petryk A and Pu WT. WT1 regulates epicardial epithelial to mesenchymal transition through beta-catenin and retinoic acid signaling pathways. *Dev Biol*. 2011;356:421-31.

85.Kovacic JC, Mercader N, Torres M, Boehm M and Fuster V. Epithelial-to-mesenchymal and endothelial-to-mesenchymal transition: from cardiovascular development to disease. *Circulation*. 2012;125:1795-808.

86.Hulshoff MS, Xu X, Krenning G and Zeisberg EM. Epigenetic Regulation of Endothelial-to-Mesenchymal Transition in Chronic Heart Disease. *Arterioscler Thromb Vasc Biol*. 2018;38:1986-1996.

87.Kanai H, Tanaka T, Aihara Y, Takeda S, Kawabata M, Miyazono K, Nagai R and Kurabayashi M. Transforming growth factor-beta/Smads signaling induces transcription of the cell type-restricted ankyrin repeat protein CARP gene through CAGA motif in vascular smooth muscle cells. *Circ Res*. 2001;88:30-6.

88.Bruno A, Mortara L, Baci D, Noonan DM and Albini A. Myeloid Derived Suppressor Cells Interactions With Natural Killer Cells and Pro-angiogenic Activities: Roles in Tumor Progression. *Front Immunol*. 2019;10:771.

89.Ongusaha PP, Kwak JC, Zwible AJ, Macip S, Higashiyama S, Taniguchi N, Fang L and Lee SW. HB-EGF is a potent inducer of tumor growth and angiogenesis. *Cancer Res*. 2004;64:5283-90.

90.Chen HI, Sharma B, Akerberg BN, Numi HJ, Kivela R, Saharinen P, Aghajanian H, McKay AS, Bogard PE, Chang AH, Jacobs AH, Epstein JA, Stankunas K, Alitalo K and Red-Horse K. The sinus venosus contributes to coronary vasculature through VEGFC-stimulated angiogenesis. *Development*. 2014;141:4500-12.

91.Hemmrich K, Suschek CV, Lerzynski G and Kolb-Bachofen V. iNOS activity is essential for endothelial stress gene expression protecting against oxidative damage. *J Appl Physiol (1985)*. 2003;95:1937-46.

92.Phng LK, Potente M, Leslie JD, Babbage J, Nyqvist D, Lobov I, Ondr JK, Rao S, Lang RA, Thurston G and Gerhardt H. Nrarp coordinates endothelial Notch and Wnt signaling to control vessel density in angiogenesis. *Dev Cell*. 2009;16:70-82.

93.Osei-Owusu P, Sabharwal R, Kaltenbronn KM, Rhee MH, Chapleau MW, Dietrich HH and Blumer KJ. Regulator of G protein signaling 2 deficiency causes endothelial dysfunction and impaired endothelium-derived hyperpolarizing factor-mediated relaxation by dysregulating Gi/o signaling. *J Biol Chem*. 2012;287:12541-9.

94.Nitta T, Hata M, Gotoh S, Seo Y, Sasaki H, Hashimoto N, Furuse M and Tsukita S. Size-selective loosening of the blood-brain barrier in claudin-5-deficient mice. *J Cell Biol*. 2003;161:653-60.

95.Puputti M, Tynninen O, Pernila P, Salmi M, Jalkanen S, Paetau A, Sihto H and Joensuu H. Expression of KIT receptor tyrosine kinase in endothelial cells of juvenile brain tumors. *Brain Pathol*. 2010;20:763-70.

96.Ko YC, Chien HF, Jiang-Shieh YF, Chang CY, Pai MH, Huang JP, Chen HM and Wu CH. Endothelial CD200 is heterogeneously distributed, regulated and involved in immune cell-endothelium interactions. *J Anat*. 2009;214:183-95.

97.Kanady JD, Dellinger MT, Munger SJ, Witte MH and Simon AM. Connexin37 and Connexin43 deficiencies in mice disrupt lymphatic valve development and result in lymphatic disorders including lymphedema and chylothorax. *Dev Biol*. 2011;354:253-66.

98.Fang JS, Coon BG, Gillis N, Chen Z, Qiu J, Chittenden TW, Burt JM, Schwartz MA and Hirschi KK. Shear-induced Notch-Cx37-p27 axis arrests endothelial cell cycle to enable arterial specification. *Nat Commun*. 2017;8:2149.

99.Ramasamy SK, Kusumbe AP, Wang L and Adams RH. Endothelial Notch activity promotes angiogenesis and osteogenesis in bone. *Nature*. 2014;507:376-380.

100.Kang HW, Walvick R and Bogdanov A, Jr. In vitro and In vivo imaging of antivasculogenesis induced by Noggin protein expression in human venous endothelial cells. *FASEB J*. 2009;23:4126-34.

101.Oda N, Abe M and Sato Y. ETS-1 converts endothelial cells to the angiogenic phenotype by inducing the expression of matrix metalloproteinases and integrin beta3. *J Cell Physiol*. 1999;178:121-32.

102.Wei G, Srinivasan R, Cantemir-Stone CZ, Sharma SM, Santhanam R, Weinstein M, Muthusamy N, Man AK, Oshima RG, Leone G and Ostrowski MC. Ets1 and Ets2 are required for endothelial cell survival during embryonic angiogenesis. *Blood*. 2009;114:1123-30.

103.Kitagawa M, Hojo M, Imayoshi I, Goto M, Ando M, Ohtsuka T, Kageyama R and Miyamoto S. Hes1 and Hes5 regulate vascular remodeling and arterial specification of endothelial cells in brain vascular development. *Mech Dev*. 2013;130:458-66.

104.Hynes RO and Yamada KM. Fibronectins: multifunctional modular glycoproteins. *J Cell Biol*. 1982;95:369-77.

105.Bork P and Doolittle RF. Proposed acquisition of an animal protein domain by bacteria. *Proc Natl Acad Sci U S A*. 1992;89:8990-4.

106.Ponting C, Schultz J and Bork P. SPRY domains in ryanodine receptors (Ca(2+)-release channels). *Trends Biochem Sci*. 1997;22:193-4.

107.Cazes A, Galaup A, Chomel C, Bignon M, Brechot N, Le Jan S, Weber H, Corvol P, Muller L, Germain S and Monnot C. Extracellular matrix-bound angiopoietin-like 4 inhibits endothelial cell adhesion, migration, and sprouting and alters actin cytoskeleton. *Circ Res*. 2006;99:1207-15.

108.Wen D, Liu D, Tang J, Dong L, Liu Y, Tao Z, Wan J, Gao D, Wang L, Sun H, Fan J and Wu W. Malic enzyme 1 induces epithelial-mesenchymal transition and indicates poor prognosis in hepatocellular carcinoma. *Tumour Biol*. 2015;36:6211-21.

109.Wang T, Chen X, Qiao W, Kong L, Sun D and Li Z. Transcription factor E2F1 promotes EMT by regulating ZEB2 in small cell lung cancer. *BMC Cancer*. 2017;17:719.

110.Fu Y, Chang A, Chang L, Niessen K, Eapen S, Setiadi A and Karsan A. Differential regulation of transforming growth factor beta signaling pathways by Notch in human endothelial cells. *J Biol Chem*. 2009;284:19452-62.

111.Bian T, Zheng L, Jiang D, Liu J, Zhang J, Feng J, Zhang Q, Qian L, Qiu H, Liu Y and Yao S. Overexpression of fibronectin type III domain containing 3B is correlated with epithelial-mesenchymal transition and predicts poor prognosis in lung adenocarcinoma. *Exp Ther Med*. 2019;17:3317-3326.

112.Delmar M and McKenna WJ. The cardiac desmosome and arrhythmogenic cardiomyopathies: from gene to disease. *Circ Res*. 2010;107:700-14.

113.Shahbazi J, Lock R and Liu T. Tumor Protein 53-Induced Nuclear Protein 1 Enhances p53 Function and Represses Tumorigenesis. *Front Genet*. 2013;4:80.

114.Helmke A, Casper J, Nordlohne J, David S, Haller H, Zeisberg EM and von Vietinghoff S. Endothelial-to-mesenchymal transition shapes the atherosclerotic plaque and modulates macrophage function. *FASEB J*. 2019;33:2278-2289.

115.Zeng L, Zampetaki A, Margariti A, Pepe AE, Alam S, Martin D, Xiao Q, Wang W, Jin ZG, Cockerill G, Mori K, Li YS, Hu Y, Chien S and Xu Q. Sustained activation of XBP1 splicing leads to endothelial apoptosis and atherosclerosis development in response to disturbed flow. *Proc Natl Acad Sci U S A*. 2009;106:8326-31.

116.Myllarniemi M, Tikkanen J, Hulmi JJ, Pasternack A, Sutinen E, Ronty M, Lepparanta O, Ma H, Ritvos O and Koli K. Upregulation of activin-B and follistatin in pulmonary fibrosis - a translational study using human biopsies and a specific inhibitor in mouse fibrosis models. *BMC Pulm Med*. 2014;14:170.

117.Horrillo A, Porras G, Ayuso MS and Gonzalez-Manchon C. Loss of endothelial barrier integrity in mice with conditional ablation of podocalyxin (Podxl) in endothelial cells. *Eur J Cell Biol*. 2016;95:265-76.

118.Abdel-Malak NA, Mofarrahi M, Mayaki D, Khachigian LM and Hussain SN. Early growth response-1 regulates angiopoietin-1-induced endothelial cell proliferation, migration, and differentiation. *Arterioscler Thromb Vasc Biol*. 2009;29:209-16.

119.Magrini E, Villa A, Angiolini F, Doni A, Mazzarol G, Rudini N, Maddaluno L, Komuta M, Topal B, Prenen H, Schachner M, Confalonieri S, Dejana E, Bianchi F, Mazzone M and Cavallaro U. Endothelial deficiency of L1 reduces tumor angiogenesis and promotes vessel normalization. *J Clin Invest*. 2014;124:4335-50.

120.Mizee MR, Wooldrik D, Lakeman KA, van het Hof B, Drexhage JA, Geerts D, Bugiani M, Aronica E, Mebius RE, Prat A, de Vries HE and Reijerkerk A. Retinoic acid induces blood-brain barrier development. *J Neurosci*. 2013;33:1660-71.

121.Weckler N, Leitzbach D, Kalinowski L, Malinski T, Busch AE and Linz W. Effect of chronic treatment with the vasopeptidase inhibitor AVE 7688 and ramipril on endothelial function in atherogenic diet rabbits. *J Renin Angiotensin Aldosterone Syst*. 2003;4:191-6.

122.Bostrom KI, Yao J, Guihard PJ, Blazquez-Medela AM and Yao Y. Endothelial-mesenchymal transition in atherosclerotic lesion calcification. *Atherosclerosis*. 2016;253:124-127.

123.Li J, Bowens N, Cheng L, Zhu X, Chen M, Hannenhalli S, Cappola TP and Parmacek MS. Myocardin-like protein 2 regulates TGFbeta signaling in embryonic stem cells and the developing vasculature. *Development*. 2012;139:3531-42.

124.Monkley SJ, Kostourou V, Spence L, Petrich B, Coleman S, Ginsberg MH, Pritchard CA and Critchley DR. Endothelial cell talin1 is essential for embryonic angiogenesis. *Dev Biol*. 2011;349:494-502.

125.Battegay EJ, Rupp J, Iruela-Arispe L, Sage EH and Pech M. PDGF-BB modulates endothelial proliferation and angiogenesis in vitro via PDGF beta-receptors. *J Cell Biol*. 1994;125:917-28.

126.Granata R, Trovato L, Lupia E, Sala G, Settanni F, Camussi G, Ghidoni R and Ghigo E. Insulin-like growth factor binding protein-3 induces angiogenesis through IGF-I- and SphK1-dependent mechanisms. *J Thromb Haemost*. 2007;5:835-45.

127.Gong Y, Yang X, He Q, Gower L, Prudovsky I, Vary CP, Brooks PC and Friesel RE. Sprouty4 regulates endothelial cell migration via modulating integrin beta3 stability through c-Src. *Angiogenesis*. 2013;16:861-75.

128.Taylor SH, Yeung CY, Kalson NS, Lu Y, Zigrino P, Starborg T, Warwood S, Holmes DF, Canty-Laird EG, Mauch C and Kadler KE. Matrix metalloproteinase 14 is required for fibrous tissue expansion. *Elife*. 2015;4:e09345.

129.Bhattacharyya S, Wang W, Morales-Nebreda L, Feng G, Wu M, Zhou X, Lafyatis R, Lee J, Hinchcliff M, Feghali-Bostwick C, Lakota K, Budinger GR, Raparia K, Tamaki Z and Varga J. Tenascin-C drives persistence of organ fibrosis. *Nat Commun*. 2016;7:11703.

130.Ummarino D. Systemic sclerosis: Tenascin C perpetuates tissue fibrosis. *Nat Rev Rheumatol*. 2016;12:375.

131.Valiente-Alandi I, Potter SJ, Salvador AM, Schafer AE, Schips T, Carrillo-Salinas F, Gibson AM, Nieman ML, Perkins C, Sargent MA, Huo J, Lorenz JN, DeFalco T, Molkentin JD, Alcaide P and Blaxall BC. Inhibiting Fibronectin Attenuates Fibrosis and Improves Cardiac Function in a Model of Heart Failure. *Circulation*. 2018;138:1236-1252.

132.Wang Z, Divanyan A, Jourd'heuil FL, Goldman RD, Ridge KM, Jourd'heuil D and Lopez-Soler RI. Vimentin expression is required for the development of EMT-related renal fibrosis following unilateral ureteral obstruction in mice. *Am J Physiol Renal Physiol*. 2018;315:F769-F780.

133.Mongiat M, Ligresti G, Marastoni S, Lorenzon E, Doliana R and Colombatti A. Regulation of the extrinsic apoptotic pathway by the extracellular matrix glycoprotein EMILIN2. *Mol Cell Biol*. 2007;27:7176-87.

134.Schiavinato A, Keene DR, Imhof T, Doliana R, Sasaki T and Sengle G. Fibulin-4 deposition requires EMILIN-1 in the extracellular matrix of osteoblasts. *Sci Rep*. 2017;7:5526.

135.Cooley BC, Nevado J, Mellad J, Yang D, St Hilaire C, Negro A, Fang F, Chen G, San H, Walts AD, Schwartzbeck RL, Taylor B, Lanzer JD, Wragg A, Elagha A, Beltran LE, Berry C, Feil R, Virmani R, Ladich E, Kovacic JC and Boehm M. TGF-beta signaling mediates

endothelial-to-mesenchymal transition (EndMT) during vein graft remodeling. *Sci Transl Med*. 2014;6:227ra34.

136.Man S, Sanchez Duffhues G, Ten Dijke P and Baker D. The therapeutic potential of targeting the endothelial-to-mesenchymal transition. *Angiogenesis*. 2019;22:3-13.

137.Luna-Zurita L, Prados B, Grego-Bessa J, Luxan G, del Monte G, Benguria A, Adams RH, Perez-Pomares JM and de la Pompa JL. Integration of a Notch-dependent mesenchymal gene program and Bmp2-driven cell invasiveness regulates murine cardiac valve formation. *J Clin Invest*. 2010;120:3493-507.

138.Azuma A, Takahashi S, Nose M, Araki K, Araki M, Takahashi T, Hirose M, Kawashima H, Miyasaka M and Kudoh S. Role of E-selectin in bleomycin induced lung fibrosis in mice. *Thorax*. 2000;55:147-52.

139.Kant S, Freytag B, Herzog A, Reich A, Merkel R, Hoffmann B, Krusche CA and Leube RE. Desmoglein 2 mutation provokes skeletal muscle actin expression and accumulation at intercalated discs in murine hearts. *J Cell Sci*. 2019;132.

140.Nasarre P, Gemmill RM, Potiron VA, Roche J, Lu X, Baron AE, Korch C, Garrett-Mayer E, Lagana A, Howe PH and Drabkin HA. Neuropilin-2 Is upregulated in lung cancer cells during TGF-beta1-induced epithelial-mesenchymal transition. *Cancer Res*. 2013;73:7111-21.

141.Lassalle P, Molet S, Janin A, Heyden JV, Tavernier J, Fiers W, Devos R and Tonnel AB. ESM-1 is a novel human endothelial cell-specific molecule expressed in lung and regulated by cytokines. *J Biol Chem*. 1996;271:20458-64.

142.Rocha SF, Schiller M, Jing D, Li H, Butz S, Vestweber D, Biljes D, Drexler HC, Nieminen-Kelha M, Vajkoczy P, Adams S, Benedito R and Adams RH. Esm1 modulates endothelial tip cell behavior and vascular permeability by enhancing VEGF bioavailability. *Circ Res*. 2014;115:581-90.

143.De Freitas Caires N and Lassalle P. Highlight on mouse endocan. *Circ Res*. 2015;116:e69-70.

144.Sidney LE, Branch MJ, Dunphy SE, Dua HS and Hopkinson A. Concise review: evidence for CD34 as a common marker for diverse progenitors. *Stem Cells*. 2014;32:1380-9.

145.Friedrich EB, Walenta K, Scharlau J, Nickenig G and Werner N. CD34-/CD133+/VEGFR-2+ endothelial progenitor cell subpopulation with potent vasoregenerative capacities. *Circ Res*. 2006;98:e20-5.

146.Tian H, McKnight SL and Russell DW. Endothelial PAS domain protein 1 (EPAS1), a transcription factor selectively expressed in endothelial cells. *Genes Dev*. 1997;11:72-82.

147.Saharinen P, Eklund L and Alitalo K. Therapeutic targeting of the angiopoietin-TIE pathway. *Nat Rev Drug Discov*. 2017;16:635-661.

148.Benezra R, Rafii S and Lyden D. The Id proteins and angiogenesis. *Oncogene*. 2001;20:8334-41.

149.Coulthard MG, Morgan M, Woodruff TM, Arumugam TV, Taylor SM, Carpenter TC, Lackmann M and Boyd AW. Eph/Ephrin signaling in injury and inflammation. *Am J Pathol*. 2012;181:1493-503.

150.Dallinga MG, Yetkin-Arik B, Kayser RP, Vogels IMC, Nowak-Sliwinska P, Griffioen AW, van Noorden CJF, Klaassen I and Schlingemann RO. IGF2 and IGF1R identified as novel tip cell genes in primary microvascular endothelial cell monolayers. *Angiogenesis*. 2018;21:823-836.

151.Kovacevic I, Muller M, Kojonazarov B, Ehrke A, Randriamboavonjy V, Kohlstedt K, Hindemith T, Schermuly RT, Fleming I, Hoffmeister M and Oess S. The F-BAR Protein NOSTRIN Dictates the Localization of the Muscarinic M3 Receptor and Regulates Cardiovascular Function. *Circ Res*. 2015;117:460-9.

152.Inoue M, Ishida T, Yasuda T, Toh R, Hara T, Cangara HM, Rikitake Y, Taira K, Sun L, Kundu RK, Quertermous T and Hirata K. Endothelial cell-selective adhesion molecule modulates atherosclerosis through plaque angiogenesis and monocyte-endothelial interaction. *Microvasc Res*. 2010;80:179-87.

153.Chen LC, Chen CC, Liang Y, Tsang NM, Chang YS and Hsueh C. A novel role for TNFAIP2: its correlation with invasion and metastasis in nasopharyngeal carcinoma. *Mod Pathol*. 2011;24:175-84.

154.Doddapattar P, Dhanesha N, Chorawala MR, Tinsman C, Jain M, Nayak MK, Staber JM and Chauhan AK. Endothelial Cell-Derived Von Willebrand Factor, But Not Platelet-Derived, Promotes Atherosclerosis in Apolipoprotein E-Deficient Mice. *Arterioscler Thromb Vasc Biol*. 2018;38:520-528.

155.Stenmark KR, Frid M and Perros F. Endothelial-to-Mesenchymal Transition: An Evolving Paradigm and a Promising Therapeutic Target in PAH. *Circulation*. 2016;133:1734-7.

156.Hardy SA, Mabotuwana NS, Murtha LA, Coulter B, Sanchez-Bezanilla S, Al-Omary MS, Senanayake T, Loering S, Starkey M, Lee RJ, Rainer PP, Hansbro PM and Boyle AJ. Novel role of extracellular matrix protein 1 (ECM1) in cardiac aging and myocardial infarction. *PLoS One*. 2019;14:e0212230.

157.Liu H, Kennard S and Lilly B. NOTCH3 expression is induced in mural cells through an autoregulatory loop that requires endothelial-expressed JAGGED1. *Circ Res*. 2009;104:466-75.

158.Goldsmith EC, Zhang X, Watson J, Hastings J and Potts JD. The collagen receptor DDR2 is expressed during early cardiac development. *Anat Rec (Hoboken)*. 2010;293:762-9.

159.Lilly AJ, Mazan A, Scott DA, Lacaud G and Kouskoff V. SOX7 expression is critically required in FLK1-expressing cells for vasculogenesis and angiogenesis during mouse embryonic development. *Mech Dev*. 2017;146:31-41.

160.Romagnani P, Lasagni L, Annunziato F, Serio M and Romagnani S. CXC chemokines: the regulatory link between inflammation and angiogenesis. *Trends Immunol*. 2004;25:201-9.